Hypoxia-Inducible Factor-1 activated by PIM1 assembles a non-canonical transcription complex and resultant regulon that drives progression of JAK2V617F myeloproliferative neoplasms

David Kealy[1,2‡], Ruth Ellerington[1,2‡], Suraj Bansal[3,4], Andy G.X. Zeng[3,4], Jessie J.F. Medeiros[3,4], Katie A. West[1,2], Nicole-Mae Blacknell[1,2], Catherine A. Hawley[1,2], Jakub Lukaszonek[1,2], Richard Gawne[2,6], Hwei Minn Khoo[7], Gillian Caalim[1,2], Bryce Drylie[1,2,5], Jenny Chatzigerou[1,2], Bianca Rodriguez Lima Ferreira[1,2], Adele K Fielding[1,2], Guanlin Wang[7,8,9,10], David G. Kent[1,2], Bethan Psaila[7,11], Adam Wilkinson[7], Andrew N. Holding[2,6], Ian S. Hitchcock[1,2], Andrew S. Mason[2,6], Vikas Gupta[3], John E. Dick[3,4] and Katherine S. Bridge[1,2]*

1 Centre for Blood Research, University of York; York, United Kingdom

2 York Biomedical Research Institute, University of York; York, United Kingdom

3 Princess Margaret Cancer Centre, University Health Network; Toronto, Canada

4 University of Toronto; Toronto, Canada

5 Barts Cancer Institute, Queen Mary University of London; London, UK

6 Jack Birch Unit for Molecular Carcinogenesis, University of York; York, UK

7 Hull York Medical School,

7 Medical Research Council Weatherall Institute of Molecular Medicine (MRC WIMM) and NIHR Biomedical Research Centre Haematology Theme; University of Oxford; Oxford, UK

8 MRC WIMM Centre for Computational Biology, University of Oxford; Oxford, United Kingdom

9 Shanghai Key Laboratory of Metabolic Remodeling and Health, Institute of Metabolism and Integrative Biology; Fudan University, Shanghai, China

10 Qizhi Institute, Shanghai, China

11 Oxford University Hospitals NHS Trust; Oxford, UK

‡ These authors contributed equally

*Correspondence to katherine.bridge@york.ac.uk

Abstract

Hypoxia-inducible factors (HIFs) are master transcriptional regulators, central to physiological oxygen homeostasis and cellular survival under limited oxygen conditions (hypoxia) and are frequently activated within malignancy. The context within which HIFs are activated significantly impacts their role within oncogenesis; this is particularly evident within acute myeloid leukaemia (AML), where HIF-1 has been characterised as both oncogenic and tumour suppressive. The mechanisms that regulate these disparities are not well understood. We therefore sought to determine whether the modality of HIF-1 activation determines its function, applying the JAK2V617F (JVF) model of myeloproliferative neoplasms (MPNs) in which HIF-1 is stabilised under normal oxygen (normoxic) conditions and is oncogenic. First, we identify that HIF-1 is stabilised in JVF cells downstream of disproportionate STAT1/5 signalling and increased expression of PIM1. Inhibition of PIM1 kinase activity eradicates HIF-1 from normoxic JVF cells. We identify a novel phosphorylation couplet (T498/S500) within the oxygen dependent degradation (ODD) domain of HIF-1 phosphorylated in JVF cells that inhibits normoxic proteasomal degradation. Applying a single-input dual-omics output chromatin interactome methodology (MinatuRIME) in matched isogenic cell lines, we identify distinct transcriptional cofactors for HIF-1 in JVF cells and redistribution of HIF-1 across the genome, indicative of JVF HIF-1 performing pre-mRNA imprinting and aberrant transcriptional control. JVF-HIF-1 produces a non-canonical target gene signature that is differentially expressed in primary mouse and human JVF haematopoietic stem and progenitor cells (HPSCs). Analysing a cohort of 298 JVF-positive MPN patients, we observe significant association of the JVF-HIF signature- but strikingly not the hypoxia-induced HIF-1 signature- with disease severity, progression, and survival of these patients. Finally, we identify a core set of 13 genes within the JVF-HIF-1 signature whose differential expression is significantly associated with spontaneous transformation of MPNs to acute myeloid leukaemia (AML). These findings demonstrate that the context and modality of HIF-1 activation can substantially alter its transcriptional function and restore the potential for targeted HIF therapies that can delineate its activity co-opted by malignancy from its essential roles within physiological oxygen homeostasis.

Introduction

Hypoxia-inducible factors (HIFs) are the major transcriptional regulators of cellular oxygen homeostasis. By coordinating both cellular and systemic responses to limited oxygen (hypoxia), the HIF regulon functions to conserve intracellular molecular oxygen and enhance delivery of exogenous oxygen to a hypoxic cell. Whilst critical to the physiological response to hypoxic exposure of normal cells, the transcriptional reach of HIFs provides a competitive advantage to cancer cells within hypoxic microenvironments such as those within solid tumours or in the bone marrow, or in malignant cells that activate HIF function by oncogenic signalling in normal oxygen (normoxic) conditions.

Under normal oxygen conditions, prolyl hydroxylase domain proteins (PHDs) hydroxylate two highly conserved proline residues on HIF-1α (Pro402 and Pro564), resulting in its recognition by the von Hippel-Lindau (VHL) E3 ligase complex, ubiquitination, and degradation by the proteasome[3]. During hypoxia, limited oxygen inhibits PHD activity, and stabilised HIF-1α protein translocates to the nucleus; the resulting heterodimerisation with the constitutively expressed HIF-1β/ARNT [2] forms an active transcription complex that binds to hypoxia-response elements (HREs) within target gene promoters[4]. The ensuing recruitment of transcription coactivators - most notably CBP/p300- forms an active transcription complex, initiating the activation of a wide array of genes involved in the response to hypoxia.

In both solid and haematological malignancies, HIFs are overexpressed as a result of two major factors: by hypoxic conditions - such as tumour or bone marrow microenvironments- and by genetic mutations, including those within *VHL*, *p53*, *Bcl2*, *Myc*, *Ras* and *JAK* (Malkov, Lee and Taylor, 2021). Whilst overexpression of the two predominant HIF isoforms (HIF-1, HIF-2) is widely observed, HIF-2 is demonstrated as almost exclusively oncogenic, whereas HIF-1 can confer either oncogenic or tumour suppressive functions (Keith, Johnson and Simon, 2011; Ortmann, 2024). This is particularly evident in myeloid neoplasia; in mouse models, inhibition of HIF-1 has been demonstrated as efficacious for treatment of myeloproliferative neoplasms (MPNs) (Baumeister *et al.*, 2020), whereas activation of HIF-1 was recently shown as efficacious for treatment of acute myeloid leukaemia (AML) (Lawson *et al.*, 2024). In agreement with these contradictory results, high levels of HIF-1α have paradoxically been associated with both the best and worst patient disease outcomes in AML[51,52] whilst beyond leukaemia, pan-cancer analysis demonstrates that only 1.8% of HIF-1/-2 target genes are conserved across 6 cancer cell lines in response to hypoxia (Lombardi et al. 2022). The underpinning mechanisms that orchestrate the multiplicity of HIF-1 within malignancy remain to be well characterised.

Contextual 'reprogramming' of transcriptional regulators as contributors to pathogenesis has previously been reported in various haematological malignancies. For example, EVI1 activation in AML by chromosome 3q26/MECOM rearrangements has been demonstrated to activate the transcriptional repressors CTBP1 and 2 in a fashion indispensable to leukaemic transformation (Pastoors et al. 2023). Furthermore, in a similar modality to HIF-1, the transcription factor WT1 (an essential regulator of genes involved in healthy haematopoiesis) appears capable of behaving as both an oncogene and tumour suppressor in AML depending on disease context, behaving as an oncogene when aberrantly expressed, and a tumour suppressor gene when mutated (Niktoreh et al. 2023).

HIF itself has also been shown to be 'reprogrammed' indirectly in malignant disease. For example, in APL, the oncogenic fusion protein PML-RARα cooperates with HIF-1α to activate a pro-leukemogenic program of HIF gene signature upregulation independent of HIF mutation (Coltella et al. 2014). Furthermore, the renal tissue specificity of clear cell renal carcinoma has been shown to be mediated by the recruitment of HIF-2α to the lineage transcription factor PAX8 as triggered by VHL protein loss (Patel et al. 2022).

To reconcile the evident context-specificity of HIF-1 activity within malignant haematopoiesis, we sought to determine whether the mechanism of HIF-1 activation determines its function. The JAK2V617F (JVF) point mutation is highly prevalent within philadelphia chromosome negative myeloproliferative neoplasms (MPNs) and is carried by >95% of patients with polycythaemia vera (PV), 50-60% of patients with essential thrombocythemia (ET) and primary myelofibrosis (PMF). Several studies have shown that in JVF-mutant MPNs, levels of HIF-1α are dramatically raised; treatment of these cells with the JAK inhibitor Ruxolitinib causes HIF-1 levels to return to normal (Baumeister *et al.*, 2020).

Herein, we provide evidence that the context and subsequent modality of HIF-1 activation directs its function: PIM1-mediated stabilisation of HIF-1α downstream of JVF signalling significantly alters the formation and function of HIF-1 transcription complexes compared to hypoxic activation, enacting a JVF-specific HIF1 regulon that is significantly associated with disease progression and survival of JVF MPN patients.

Results

HIF-1α is stabilised in JAK2V617F cells downstream of disproportionately activated STAT1/STAT5 signalling and increased PIM1 kinase expression

We first sought to determine whether stabilisation of HIF-1α protein, previously reported in the *jak2v617f*-transduced 32D murine cell line (Baumeister *et al.*, 2020), was detectable across other relevant JVF mutant cell line models. Immunoblot analysis of the murine pro-B

cell line hMPL BaF3 (Palacios and Stenmetz, Koga et al.), the human leukaemic megakaryocytic cell line UT7/TPO (Komatsu et al 1996), the human JVF mutation heterozygous transformed essential thrombocytopenia megakaryoblastic line SET2 (Uozumi et al., Zhao et al. 2012) and the human erythroleukaemic erythroblastic JVF mutation homozygous line HEL (Martin and Papayanopolou) all demonstrated elevated HIF-1α levels at 20% O_2 (normoxia) compared to corresponding wildtype JAK2 cell lines (Fig. 1A). We next employed the *ex vivo* PVA expansion culture system for murine HSCs to interrogate these findings further (Wilkinson *et al.*, 2019), as we previously demonstrated that the purity of HSC expansion cultures are enhanced by hypoxic conditions (Igarashi *et al.*, 2023). Flow cytometric analysis of HSCs expanded under normoxia (20% O_2), physioxia (5%) O_2 and hypoxia (1% O_2) demonstrated correlative levels of HIF-1α with oxygen concentrations in WT HSCs (Fig. S1(A)). Upon treatment with the HIF-1α-specific inhibitor GN44028, the percentage of LT-HSCs (CD201+ CD150+ LSK) in these populations significantly reduced across all oxygenation conditions, with a concomitant increase in percentage of lineage committed cells (Fig. S1B). We next analysed Lineage-Sca1+cKit+ (LSK) cells from JVF homozygous, heterozygous and wildtype C57/BL6 mouse bone marrow, which confirmed JVF-mediated stabilisation of HIF-1α in short-term (6h) hypoxia-exposed cells (HIF-1α levels remained below the limits of detection for all genotypes in normoxia) (Fig. 1B and Fig. S2A). Western blot analysis of LSK lysate further confirmed these findings (Fig. S2B).

We next undertook *ex vivo* expansion culture of JVF homozygous, heterozygous and wildtype long-term HSCs, and first discovered that expansion of LT-HSCs from homozygous JVF mice was not supported by this system. We hypothesise this may be due to saturation of the JAK/STAT signalling pathway because of supraphysiological levels of TPO within the culture conditions, although this is yet to be fully interrogated. However, we observed significant differences in lineage committal decisions of heterozygous JVF HSCs in expansion cultures, with a significant reduction in the proportion of Lin- Sca1+ cKit+ (LSK) HSPCs in JVF heterozygous populations and a corresponding increase in the proportion of progenitors (Lin^- $Sca1^-$ $cKit^+$; Prog) (Fig. S3A-B) in keeping with immunophenotypes observed from fresh bone marrow from these mice (Li *et al.*, 2014). Expansion cultures performed under a dose-range of GN44028 (HIF-1 inhibitor) demonstrated indiscriminate inhibition of the proportion of LSKs within the cultures, regardless of phenotype, although it did confer disease-beneficial effects on the expanded progenitor population from JVF heterozygous cultures. These findings resonate with the effects of the antibiotic Echinomycin (also an inhibitor of HIFs) which inhibited proliferation of 32D cells indiscriminately of JVF-mutation status, and deleteriously increased the colony-formation capacity of healthy CD34+ peripheral blood mononuclear cells (PBMCs) (Baumeister *et al.*, 2020). Taken together,

these data demonstrated a central role of HIF-1 within both normal and JVF-mediated malignant haematopoiesis, and therefore underscored the importance of delineating HIF-1 function in each of these settings for potential viable therapeutic strategies for JVF-MPN disease. It was therefore critical to define the mechanism of HIF activation within the JVF context.

In JVF-32D cells, elevated levels of normoxic HIF-1α detected by Baumeister et al. were attributed to increased levels of intracellular ROS (Baumeister et al. 2020), acting to stabilise HIF via activation of PI3K/AKT signalling (Marty et al. 2013). This was demonstrated by the application of the indirect ROS inhibitor DMF, triggering a reversal in observed HIF-1α stabilisation. Furthermore, current understanding of canonical TPO-mediated HIF-1α stabilisation suggests that TPO binding to MPL receptor triggers HIF-1α stabilisation through JAK2 signalling-induced ROS generation (Yoshida et al. 2008). We therefore applied the ROS-scavenger NAC to our panel of JVF-mutant immortalised cell lines to see if ROS-induced HIF-1α stabilisation could be recapitulated. Interestingly, we did not observe NAC-induced destabilisation of HIF-1α protein (Fig. 1C and Fig. S4A), however upon treatment with DMF, destabilisation of JVF-HIF-1α did occur (Fig. S4B). The greater specificity and complete ablation of ROS via the scavenging effect of NAC suggest that ROS are in fact not responsible for the observed stabilisation of HIF-1α, and that the destabilising effect of DMF on JVF-HIF-1α is instead likely due to ROS-independent mechanisms.

ERK1/2 kinase activity has been shown to be elevated in the presence of the JVF mutation (Levine et al. 2005). Furthermore, it has been well established that ERK1/2-mediated phosphorylation of HIF-1α at sites S641/S643 promotes HIF-1α nuclear accumulation and is essential for HIF-1 transcription activity in hypoxia (Koukoulas et al. 2021). We therefore sought to investigate the possible role of ERK1/2 in JVF-mediated HIF-1α stabilisation. Application of the specific ERK1/2 kinase-activity inhibitor SCH874 to UT7/TPO JVF cells failed however to affect elevated levels of HIF-1α protein (Fig. S5), suggesting that the mechanism of JVF-mediated HIF-1α stabilisation is ERK1/2-independent. Combined, these findings necessitated a novel approach to decipher the mechanism by which HIF-1α protein is stabilised in the presence of the JVF mutation.

Phosphorylation of HIF-1α at several highly conserved sites has been extensively demonstrated to critically modulate the interactome of HIF-1 and its transcriptional function (Kalousi et al. 2010, Mylonis et al. 2008, Mylonis et al. 2006) and to aid the promotion of CBP/p300 co-activator recruitment and upregulation of transcriptional activity (Gradin et al. 2002, Lancaster et al. 2004, Cho et al. 2007). We therefore reasoned that aberrant kinase activation and phosphorylation of HIF-1α downstream of JVF could be responsible for HIF-

1α stabilisation. We applied an unbiased, high-throughput barcoded phospho-flow cytometry approach (Fig. S8) to fully characterise the signalling cascades downstream of JVF compared to TPO/MPL-mediated wildtype JAK2 signalling in UT-7/TPO cells. These analyses demonstrated not only a global amplification of JAK2 signalling in JVF mutant cells but identified significant relative activation of specific kinase cascades (Fig. 1D(I)). By performing 'parts of a whole' analysis (wherein MFI values for each phospho-peptide are calculated as a fraction of total phospho-peptide MFI), we identified that STAT1 and STAT5 were disproportionally over-activated downstream of JVF, collectively representing 34.3% of the total signalling activity in JVF cells compared to 24.9% in wildtype TPO-stimulated cells (Fig. 1D(II)). We did not observe any significant change in contribution of STAT3 activation and saw an 11.9% reduction in relative ERK activation in JVF cells, thus corroborating our findings that ERK phosphorylation was not contributing to HIF-1α activation in the cells. To confirm that disproportionate STAT1/5 signalling downstream of JVF was responsible for stabilised HIF-1α protein, we treated JVF-homozygous HEL cells with a variety of STAT inhibitors and observed that STAT1 inhibition by Fludarabine triggered dramatic reduction of HIF-1α (Fig. S6).

Unlike STAT3, STAT1/5 are not known to be direct interactors of HIFs (Pawlus, Wang and Hu, 2014; Dinarello *et al.*, 2023). We therefore interrogated STAT1/5 target genes for known kinase regulators of HIF-1α TFBS - Home (systemsbiology.net), identifying 1078 common gene targets between STAT1 and STAT5 (Fig. 1E). Of these common targets, 17 kinases were identified and of these, 1 was a known kinase of HIF: the CAMK serine/threonine kinase PIM1. PIM1 is known to contribute to the pathogenesis of haematological malignancies (Mondello, Cuzzocrea and Mian, 2014) and has previously been described as phosphorylating HIF-1α at Thr455 in prostate cancer (Casillas *et al.*, 2021), stabilising HIF-1α in an oxygen-independent manner. PIM1 has also shown to be upregulated in murine HSPCs harbouring the JVF mutation (Dutta *et al.*, 2022), implicating PIM1 as a possible candidate mediating HIF-1α aberrant stabilisation.

To pursue this theory, we analysed pre-existing publicly available HSPC bulk RNAseq datasets from heterozygous JVF mice (GSE180853 (Li *et al.*, 2022)) and observed raised levels of PIM1 transcript in the LSK and megakaryocyte erythroid progenitor (MEP) cell population compared to wildtype counterparts (Fig. 1F and Fig. S7). This finding was confirmed via RT-qPCR in both whole and lineage depleted bone marrow from homozygous JVF mice where significantly higher PIM1 transcript expression compared to wildtype was observed (Fig. 1G). To confirm these findings in patients, we re-analysed myelofibrosis (MF) MPN patient scRNAseq data (Psaila *et al.*, 2020) for patients harbouring the JVF mutation, and found that not only were total levels of PIM1 transcript elevated in these patients, but

that overexpression was localised to the disease-driving expanded megakaryocyte progenitor (MkP) population (Fig. 1H). Taken together, these findings demonstrate that disproportionate activation of STAT1/5 occurring downstream of JAK2V617F upregulates PIM1 and subsequent HIF-1α stabilisation in MPN disease driving HSPCs.

PIM1 inhibition confirms JAK2V617F-induced PIM1 stabilises HIF-1α without modifying JVF signalling

To confirm PIM1-mediated HIF-1α stabilisation, we dosed both JVF and wildtype UT7/TPO and BaF3 hMPL cells with increasing concentrations of the PIM1-specific inhibitors TCS PIM1 and SMI-4a and the pan-PIM inhibitor PIM447. We observed dose-dependent decreases in HIF-1α stabilisation by immunoblot with all PIM inhibitors (Fig. 2A(I) and Fig. S9A-B), thus suggesting that PIM, and more specifically PIM1, is necessary for JVF-mediated HIF-1α stabilisation. Of the specific PIM1 inhibitors tested, SMI-4a did not tamper with levels of PIM1 protein, and thus was chosen for PIM1 inhibition investigations going forward. To contrast the effect of PIM1 inhibition with JAK inhibition on HIF-1α levels, we next applied either SMI-4a or the JAK inhibitor Ruxolitinib (Rux) to JVF and wildtype UT7/TPO cells, either starved overnight or stimulated with TPO and cultured under normoxic (20% O_2) or hypoxic (1% O_2) conditions. To analyse downstream signalling, barcoded phospho-flow cytometry was again performed. In keeping with western blot data, SMI-4a reduced HIF-1α levels in JVF cells in both normoxia and hypoxia, however we observed no effect on HIF-1α levels in WT cells stimulated with TPO in either oxygen condition (Fig. 2A(II)). In contrast, Rux-treatment caused significant downregulation of HIF-1α levels across all genotypes, and oxygen concentrations. These demonstrate that inhibition of PIM1 can confer specificity to HIF-1 inhibition downstream of JVF signalling, whilst not affecting physiological activation of HIF-1 by hypoxia or TPO.

The JAK inhibitor Ruxolitinib is currently the most common drug treatment given in JVF-positive cases of myeloproliferative neoplasia ((Quintas-Cardama et al. 2010, Ehgtedar et al. 2012, Mesa et al. 2013, Vainchenker et al. 2023). However, JAK inhibition disrupts many crucial signalling pathways within the cell, and therapeutically causes a number of poorly tolerated side effects (Boldrini et al. 2024). To investigate if PIM1 inhibition could create a more targeted downstream therapeutic approach, we treated SET2 and HEL myeloproliferative patient-derived cancer cell lines with either Ruxolitinib or SMI-4a (Fig. 2B(I)). Whilst Rux-treatment significantly downregulated signalling across all pathways analysed, SMI-4a selectively affected levels of HIF-1α. Broader analysis of signalling in JVF mutant UT7/TPO cells demonstrated inhibition of both TPO signalling in JAK2 WT cells and

oncogenic JVF signalling, whereas SMI-4a treatment did not deregulate these pathways (Fig. 2B(II) and Fig. S11).

To further investigate whether PIM1 inhibition of HIF-1α could confer disease-specific effects on JVF HSPCs, we conducted *ex vivo* expansion of long-term HSCs from wildtype and JVF heterozygous mice in the PVA culture system (Fig. 2C and Fig. S14). Of note, we found that expansion of LT-HSCs from homozygous JVF mice was not supported by this system; we hypothesise this may be due to saturation of the JAK/STAT signalling pathway as a result of supraphysiological levels of TPO within the culture conditions. We performed immunophenotyping of the culture populations after 14 days of expansion (Fig. S12-13), and observed a significant reduction in the proportion of Lin- Sca1+ cKit+ (LSK) HSPCs in JVF heterozygous populations and a corresponding increase in the proportion of progenitors (Lin^- $Sca1^-$ $cKit^+$; Prog) in keeping with the disease phenotype observed in fresh bone marrow from these mice (Li *et al.*, 2014). Expansion cultures performed under a dose-range of either HIF-1 (GN44028) or PIM1 (SMI-1a) inhibition demonstrated that PIM1 inhibition rescued the JVF heterozygous LSK/Prog phenotype, returning the LSK/Prog ratios observed in wildtype expansion cultures. Of note, we observed that HIF-1 inhibition indiscriminately inhibited the proportion of LSKs within the cultures, regardless of phenotype, although did seem to confer disease-beneficial effects on the progenitor population of JVF heterozygous cells. Taken together, these data demonstrate that HIF-1α is stabilised in JVF cells as a result of PIM1 kinase activity, and that inhibition of PIM1 can rescue aberrant HIF-1 activation and JVF signalling whilst not affecting physiological JAK or HIF activity.

HIF-1a is stabilised via phosphorylation of T498/S500 in JAK2V617F cells

PIM1 kinase has previously been shown to phosphorylate HIF-1α at the Thr455 site in prostate cancer cells (Casillas et al. 2021). This phosphorylation event inhibits the canonical hydroxylation of the oxygen dependent degradation (ODD) domain by PHD enzymes and subsequent ubiquitination and degradation under normoxic conditions, leading to HIF-1α protein stabilisation. To investigate whether a similar mechanism occurs downstream of JVF signalling, we performed an immunoblot of both wildtype and JVF UT7/TPO cells probed with a phospho-T455 HIF-1α antibody. Interestingly, decreased T455 pHIF-1α levels were detected in JVF cells relative to wildtype and treatment with the PIM1 inhibitor SMI-4a conferred no effect on HIF-1α levels (Fig. S15), suggesting that PIM1-mediated HIF-1α stabilisation in the presence of the JVF mutation is not affected via phosphorylation at the T455 site.

We therefore performed phospho-proteomic mass spectrometry analysis of UT7/TPO JVF, and wildtype cells exposed to hypoxia, enriched for phosphorylated proteins by TiO_2 and

enriched for HIF-1α via immunoprecipitation. Phosphorylation of HIF-1α in wildtype cells was detected at the canonical hypoxia/ERK sites (S641/643), whereas in the matched isogenic JVF cell line under the same hypoxic conditions, an additional phosphorylation couplet was detected at T498/S500 (Fig. 3A(I)-(II)). Interestingly, no phosphorylation at the T455 site was detected in any condition, further suggesting that the mechanism of PIM1-mediated HIF-1α stabilisation downstream of JVF is unique from that observed in prostate cancer cells. Whilst the T498 site is not well conserved, the S500 site is well conserved evolutionarily among mammals and a variety of other non-mammalian species, suggesting the importance of the S500 site as a regulatory site (Fig. 3B).

The location of the novel T498/S500 phosphorylation sites in the ODD and their proximity to the canonical normoxia-dependent hydroxylation sites at P402 and P564 (Fig. 3C) suggested to us that, whilst PIM1 was not phosphorylating HIF-1α at the same residue as in prostate cancer, perhaps the mechanism of its HIF-1α stabilisation through the inhibition of canonical ODD hydroxylation was similar. Wildtype or JVF mutant UT7/TPO cells were therefore treated with the proteasome inhibitor MG-132 in combination with SMI-4a (Fig. 3D) to assess the role of proteasomal degradation in PIM1-mediated stabilisation of HIF-1α in the presence of the JVF mutation. Combined treatment with MG-132 and SMI-4a was sufficient to re-stabilise HIF-1α levels, demonstrating that PIM1-mediated stabilisation of HIF-1α downstream of JVF signalling occurs via inhibition of canonical normoxic proteasomal degradation.

HIF-1α assembles a non-canonical transcription complex in JAK2V617F cells

Having identified that HIF-1α stabilised in JAK2V617F cells is phosphorylated at non-canonical sites, we next sought to determine whether this altered the transcriptional activity of HIF-1. HIF-1α phosphorylation is known to alter its interaction with co-regulatory proteins (In recent years, newly identified HIF transcription cofactors including TRIM28 and PAX8, identified in breast(Patel *et al.*, 2022; Yang *et al.*, 2022)) and renal cancer(Patel *et al.*, 2022), respectively, identify the existence of cancer context-specific regulators of HIF transcription activity.); we therefore wanted not only to capture the genomic loci and target genes of HIF-1 in JAK2V617F cells, but also the transcription co-regulators as potential targetable disease-specific regulators. We therefore developed a single-input dual-output chromatin-immunoprecipitation methodology called miniatuRIME, integrating the principles of ChIPseq and qPLEX-RIME (quantitative multiplexed Rapid Immunoprecipitation Mass spectrometry of Endogenous proteins), to quantitatively analyse the chromatin interactome of HIF-1α from a single sample (Fig. 4A(I)). JAK2 V617F/WT hMPL BaF3 cells were cultured at normoxia (20%) or hypoxia (1%, 6h) and chromatin immunoprecipitation against HIF-1α was

performed. First, we observed that despite equal chromatin concentrations being loaded on to ChIP columns, we observed significantly higher HIF-1α protein levels immunoprecipitated from JVF chromatin (compared to wildtype chromatin) whereas the concentration of chromatin associated with HIF-1α was significantly reduced (Fig. 4A(II)). This was particularly evident when comparing WT_Hx to VF_Nx samples, where normalised abundance of HIF-1α protein from the ChIPs was comparable, whereas the mean genomic DNA peak intensities from VF_Nx were significantly reduced compared to WT_Hx. For proteome analysis, samples were normalised against HIF-1α spectral counts to control for this variance.

Analysis of the protein interactors of HIF-1α at the chromatin in WT_Hx cells identified known co-regulator interactors including HIF-1β/ARNT, HSP90 and NCOA5 (Patel *et al.*, 2022). Analysis of HIF-1α in JVF cells under normoxia (VF_Nx) or hypoxia (VF_Hx) compared to WT_Hx identified significant differences in the interactome of HIF-1α at the chromatin. Unsurprisingly, several cofactors were identified as common between all conditions. However, notably, 15 binding partners were found to exclusively associate with HIF-1α in cells harbouring the JVF mutation, with 2 and 7 cofactors unique to JVF cells under normoxic and hypoxic conditions respectively (Fig. 4B). Differences observed between VF_Nx and VF_Hx conditions are to be expected given the significant alterations observed to the epigenome under hypoxic exposure (Batie *et al.*, 2019).

The intensity of the binding of these cofactors to HIF-1α relative to wildtype hypoxic cells was calculated and displayed in heatmap form to illustrate differential binding between conditions (Fig. 4C). This illuminated key patterns of protein association unique to JVF cells, such as an increased association with cofactor TDP-43 and decreased association with protein markers of degradation such as ubiquitin and VHL, further lending evidence to our hypothesis that HIF-1αs JVF stabilisation is due to an inhibition of hydroxylation and subsequent VHL-mediated ubiquitination.

Protein intensity relative to HIF-1α for each of the identified cofactors were ranked for each condition and those with GeoMean greater than 0.01 were retained (following exclusion of structural and non-murine proteins). These remaining proteins were subjected to STRING analysis for each condition to better understand the role and interactions of these associated proteins (Fig. 4D and Fig. S16A-B). VF_Hx HIF-1α possesses a reduced interactome, despite greater levels of HIF-1α relative to WT_Hx and VF_Nx (5.42 and 3.15-fold greater respectively), suggesting a significant alteration in HIF-1α protein confirmation in the combined presence of JVF and hypoxic conditions. Most interestingly, spliceosomal factors

were prominently and uniquely associated with JVF HIF-1α (including TDP-43, KHDRBS1/Sam68) along with ribosomal factors in normoxic treated cells.

The differential binding of cofactors revealed key cofactors unique to each condition, with a significant increase in abundance of the cofactors TDP-43 and GOLGA3 observed in both VF_Nx and VF_Hx relative to WT_Hx (Fig. 4E). Several other cofactors such as NCOA5, HSPA8, SIK2 and IMPDH were also shown to be significantly differentially bound between the conditions. Novel JVF-unique interacting partners identified through qPLEX-RIME were then validated by endogenous co-immunoprecipitation assays conducted UT-7/TPO cells expressing either wildtype JAK2 or JVF at normoxia (20% O_2) or hypoxia (1% O_2, 6 Hours) (Fig. 4F(I)-(II)). This confirmed the interaction of TDP-43, SFPQ, GOLGA3, SIK2 and IMPDH with endogenous HIF-1α, with greater IMPDH binding observed in JVF samples relative to wildtype. GOLGA3 was expressed at a higher level in JVF samples relative to wildtype, which was recapitulated in the immunoprecipitation. During our previous phosphoproteomic investigation of HIF-1α phosphorylation, the JVF-unique phosphorylation of several other proteins was also detected as being co-immunoprecipitated with HIF-1α. Most interestingly, these phosphorylated co-immunoprecipitated proteins included GOLGA3, with several distinct sites detected as phosphorylated when pulled down with HIF-1α (Fig. S17).

HIF-1 is genomically redistributed in JAK2V617F cells

Having identified a distinct set of co-regulatory transcriptional components of HIF-1 complexes in JAK2V617F cell, we next sought to determine whether the binding loci of HIF-1 throughout the genome was altered because of activation via JAK2V617F signalling. Continuing our single-input, dual output chromatin interactome approach (Fig. 5A), we interrogated the genomic sequences immunoprecipitated with the complexes analysed in Figure 4. First, we identified a largely canonical HIF-1 signature associated with HIF-1 in BaF3 cells exposed to 1% O2 for 6 hours (WT_Hx) (Fig. S18), including classical HIF-1 hypoxia signature genes *Vegfa* and *Slc2a1* (Fig. S19). Globally, we observed a reduction in median peak intensity (MPI) for HIF-1α in JAK2V617F cells (Fig. 5B, Fig. S20), marked by the emergence of a population of loci of low intensity (MPI<2), unobserved in WT_Hx condition, despite HIF-1α protein levels being higher (Fig. 4A(II)). Concomitant with this, we observed very few loci that were only bound by HIF-1α in JAK2V617F mutant cells, and the number of bound sites were reduced in these cells (Fig. S21). These data indicate that the DNA-binding capacity and/or the proximity of HIF-1α to DNA is reduced in JAK2V617F mutant cells at particular sites compared to in hypoxic WT JAK2 cells.

To calculate the priority distribution of HIF-1 across the genomic within a given cellular context, peak intensity for HIF-1 at loci was rank-scored for each condition WT_Hx, VF_Nx

and VF_Hx; Δrank-score for VF_Nx/VF_Hx was calculated to identify loci that were higher or lower ranked relative to WT_Hx. First, we observe global priority redistribution of HIF-1, with the intensity ranking of 42% and 26% of sites in VF_Nx and VF_Hx, respectively, conferring Δrank-score greater than a quartile (Fig. 5C). Analysing the chromosomal distribution of intensity ranking, a population of depreciated HIF-1 bound sites in VF_Nx were evident in chromosomes 1-4 and prioritised sites at chromosome 8 and 14 (Fig. 5D and Fig. S22); notable genetic loci losses and gains included *Usf1* and *Dusp4*, respectively (Fig. 5E). In VF_Hx cells HIF-1a binding was overall enhanced on chromosome 12 (Fig. 5D and Fig. S22); these sites included *Bag8*, *Coa8* and *Hectd1* (Fig. 5E). To determine whether chromatin accessibility alterations mediated by JAK2V617F signalling was a factor in the redistribution in HIF-1a, we cross-analysed VF_Nx/VF_Hx ChIPseq data with a JAK2V617F scATAC-Seq dataset (Fig. 5F and Fig. S23) (Izzo *et al.*, 2024). No significant difference in accessibility at HIF-1a binding loci was observed, suggesting that HIF-1a redistribution was not mediated by site accessibility. Feature analysis of HIF-1 bound loci demonstrated a 14% reduction in hypoxia-responsive elements in VF_Nx/VF_Hx compared to WT_Hx (Fig. 5G) and a modest increase in binding in intergenic regions and introns in VF_Nx cells (Fig. 5H).

JAK2VF-HIF-1 gene-signatures diverge from canonical HIF-1 targets and correlate with MPN disease progression and survival

Next, HIF-1 gene-signatures were generated from enriched binding loci in VF_Nx/VF_Hx relative to WT_Hx ($q<0.03$); a WT_Hx signature was generated relative to WT_Nx as a control canonical hypoxia signature (Fig. 6A). Gene ontology pathway analysis of the WT_Hx signature demonstrated canonical HIF-1 pathways, including glycolysis, response to oxidative stress and response to hypoxia. (Fig. 6B(I)). The VF_Nx gene-signature included non-canonical HIF-1/Hypoxia pathways including DNA metabolism, DNA damage response, and RNA processing, with a reduction of glycolysis pathways observed (Figure 6B(II)); strikingly, the VF_Hx gene-signature was even further separated in gene ontology from canonical WT_Hx (Fig. 6B(III)) pathways, with cell cycle progression and checkpoint pathway genes demonstrating the greatest contribution to the signature . Furthermore, VF_Nx and VF_Hx gene-signatures contained only 9 and 2 genes, respectively, of the HIF gene metascore - a recently identified core set of 48 HIF target genes highly conserved across cell/cancer types exposed to hypoxia (Fig. S24), underscoring the functional divergence incurred by the modality of HIF-1 activation in JAK2V617F mutant cells. (Lombardi *et al.*, 2022).

To investigate whether the redistribution of HIF-1 in response to JAK2VF signalling was reflected in the transcriptome, we next interrogated the expression of the VF_Nx and VF_Hx HIF-1 signatures in primary haematopoietic stem and progenitor cells (HSPCs) from jak2$^{wt/wt}$ and jak2$^{vf/vf}$ C57/BL6 mice (Fig. 7B) (Li *et al.*, 2022) . This analysis identified 74.6% of VF_Hx signature genes were differentially expressed in multipotent jak2$^{vf/vf}$ MEP cells, whereas only 4.6% of the signatures were differentially expressed in the more primitive LSK population. The cell type-specific activation of the HIF-1 VF_Hx signature within MEPs in mice resonates with recent findings identifying epigenetic changes in the erythroid and megakaryocytic progenitors of JAK2V617F patient samples, the cell types that undergo significant clonal expansion, that increase accessibility of particular transcription factor motifs in late erythroid progenitor populations (Izzo *et al.*, 2024). Of note, we observe that a significant proportion of differentially expressed VF_Hx signature genes were downregulated in MEPs. HIFs are not known to confer transcription-repressive functions, suggesting that peri- or post-transcriptional mechanisms mediated by HIF-1 and/or co-factors confer the observed transcript repression.

Having determined differential expression of the VF_Nx and VF_Hx signatures at the transcriptome level, we sought to determine whether adverse HIF-1 transcriptional output in response to JAK2V617F mutation conferred pathophysiological effects in MPN patients. A 298-patient cohort [need details here on RNA - what cells, when taken] with matched disease progression and survival data demonstrated a significant correlation between patients with the highest MIPPS70 disease severity classification and expression of the VF_Nx and VF_Hx signatures compared to those with intermediate disease (Fig. 6C). Disease severity was reflected in the overall survival of the cohort, for whom those in the upper median group of VF_Hx gene signature expression (VF_Hx ^{HIGH}) demonstrated significantly worse overall survival, with a median survival of 4 years compared to 8 years for VF_Hx^{LOW} patients (Fig. 6D).

JAK2V617F-activated HIF-1 target genes contribute to disease progression and outcome

To identify particular genes driving the differences observed between VF_Nx and VF_Hx signatures in patient survival, we identified the disparate genes between these signatures (158 for both VF_Nx and VF_Hx) and performed meta-analysis across human and mouse JAK2V617F ChIPseq, ATAC-Seq, transcriptomic and survival data to identify those within the VF_Hx signature with significant differential expression that also contributed to disease outcome (Figure 7A) (Psaila *et al.*, 2020; Li *et al.*, 2022). First, we observed that the JAKVF-HIF-1 target genes for which differential expression was observed both within megakaryocyte erythroid progenitors (MEPs) in jak2v617f homozygous mice (compared to

jak2 wild type mice) (Fig. S25) and also in scRNAseq within the expanded megakaryocyte progenitor population of JAK2V617F patients (compared to healthy control donors), were significantly associated with disease severity (MIPSS70 score) and overall survival of JAK2VF patients (Fig. 7C(I)-(II)). A notable pathway emergent from this analysis was the DNA damage response, with genes including proliferating cell nuclear antigen (PCNA), BLM RecQ Like Helicase (BLM), aurora kinase B (AURKB) and BCL2L1 (BCL2XL) (Fig. S26) all significantly upregulated in transcript expression in MEPs/MkP and significantly associated with disease progression and survival. JAKVF-HIF-1 genes that were globally upregulated throughout HSPC clusters, for example EIF4EBP1 (Fig. 7D), TNKS, HECTD1, WIPF1, PPID (Fig. S27) were not correlated with disease progression or survival. Finally, we noted a small cohort of genes that were significantly upregulated in more primitive progenitor populations in patients (HSPC3), that were inversely correlated with disease severity and survival, including Immediate Early Response 3 (IER3), which regulates cell cycle/apoptosis decisions (Fig. S28). These data are in keeping with previous findings that the disease-specific expanded MkP population for JAK2V617F MF patients, and also identify that HIF-1 activated downstream of JAK2V617F signalling induces DNA damage response genes that contribute to MPN disease progression and patient survival.

JAK2VF-HIF-1 regulon correlates with transformation of MPNs to AML (Figure 8)

JAK2V617F positive MPN patients who develop myelofibrosis are at risk of spontaneous conversion to acute myeloid leukaemia; the molecular mechanisms underpinning this pathobiological event are not well characterised (Dunbar, Rampal and Levine, 2020). 11 patients from the JAK2V617F MPN cohort converted to AML; we therefore analysed expression of the VF_Hx signature genes from matched pre-/post-transformation samples. No significant difference in expression of the gene signatures as a whole was observed in these patients pre-/post-transformation (Fig. S29). We therefore individually analysed expression of JAK2VF-HIF-1 target genes in these patients pre- and post-transformation, and identified the expression of 13 genes significantly altered, comprising 5 up-regulated and 8 down-regulated genes (Fig. 8A). Notably, panther pathway analysis of the upregulated genes identified the DNA damage response as a significant HIF-1 mediated pathway associated with leukemic transformation. Downregulated pathways included negative feedback of the hypoxic response (*EGLN1*) and regulators of glucose metabolism (*IER3, HK2*). Analysis of the 13-genes as a signature demonstrated an extremely strong correlation with disease progression (MIPPS70 classification), myelofibrosis (overt, post-ET and post-PV), and significantly worsened survival, (Fig 8B). These results together uncover a HIF-1 regulon in JAK2V617F mutant MPNs that drive leukaemic transformation.

Discussion

HIF-1 is a master transcriptional regulator integral to normal oxygen homeostasis in healthy cells. In the malignant setting, HIF-1 activated by microenvironmental hypoxia or aberrant signalling cascades contributes to disease progression and treatment resistance, however the directionality and potency of its role is disease-context dependent; this is particularly evident within myeloid neoplasia (REFs). We therefore sought to determine whether the modality of HIF-1 activation - either physiologically by hypoxia or pathologically as a result of oncogenic signalling- could alter its transcriptional function and role within disease pathobiology, interrogating JAK2V617F-driven MPNs as a disease model system.

Whilst JAK2V617F mutation is known to activate JAK-STAT signalling in a cytokine-independent manner, recent studies by our groups and others have revealed that structural conformation of the TPO-MPL-JAK2 complex controls downstream signalling outcomes (Tsutsumi *et al.*, 2023), and that the JAK2V617F mutation alters and strengthens the intermolecular interactions in the pseudokinase domain dimerization interface (Wilmes *et al.*, 2020). High-throughput phospho-flow cytometry reveals that STAT1 and STAT5 are disproportionately activated by JAK2V617F compared to TPO-stimulated JAK2, with relative suppression of ERK signalling. These data reveal that JAK2V617F mutation confers not only cytokine-independent JAK-STAT signalling but deregulation of this cascade, driving mutant-specific transcriptional effects via STAT1 and STAT5, upon which JAK2V617F MPNs become reliant (Yan, Hutchison and Mohi, 2012). These data provide the mechanism for recent single-cell multi-omic analyses that describe enhanced activity of STAT1/STAT5 promoters in JAK2V617F mutant patient CD34+ cells (Izzo *et al.*, 2024).

PIM1 is a direct transcriptional target of STAT1 and STAT5, and was previously described as a kinase acting upon HIF-1a in colorectal cancer. Additionally, PIM1 was identified as conferring phenotypic effect in murine and *in vitro* models of JAK2V617F malignancy (Mazzacurati *et al.*, 2015; Dutta *et al.*, 2022) and more widely has been extensively linked to haematological malignancies. Concurrent with these data, meta-analysis of murine and human RNAseq identify upregulation of PIM1 transcript, as well as direct analysis of murine BM-derived HSPCs by qRT-PCR. Mechanistically we determine that HIF-1a is stabilised in JAK2V617F cells by a PIM1 dependant mechanism through inhibition of proteasomal degradation via the PHD/VHL hydroxylation/ubiquitination couplet, the same route by which HIF-1a is stabilised by PIM1 in prostate cancer. Notably, we identify a previously undescribed phosphorylation event on HIF-1a in JAK2V617F cells occurring within the oxygen dependent degradation (ODD) domain (T498/S500), which is distinct from the

previously described PIM1 site (T455). Whilst well-characterised in terms of post-translational modifications and interactors, the ODD domain of HIF-1a is inherently unstructured. This is a typical feature of transcription factors to enable their function to be pliable in response to co-regulator protein interactors. Phosphorylation of the T498/S500 sites might sterically block interaction of PHD enzymes, however their proximity to the hydroxy-target proline residues (P402/P564) indicates an intermediate conformational alteration or protein interaction may be involved. Further studies are warranted to determine the effects of T498/S500 phosphorylation on HIF-1a structure and function in JAK2V617F MPNs, and also to identify if this pathological phosphorylation event occurs in haematological or solid cancers of other origin.

Despite its potency within malignant transformation and progression, pharmacological inhibition of HIFs has been largely unsuccessful, with the exception of the recent FDA-approved HIF-2a inhibitor Belzutifan (MK-6482), indicated for advanced clear cell renal cell carcinoma (Center for Drug Evaluation and Research, 2023). Unlike HIF-1a, the HIF-2a isoform is exclusively oncogenic in a malignant context, suggesting that its regulation is less context-specific. HIF-1a inhibition, conversely, has not been successful as a therapeutic avenue in malignancy, largely due to the negative side effects of impaired canonical HIF activity in healthy cells (Ban et al. 2021, Fallah and Rini 2019). The ability to delineate physiological from pathological activation or function of HIF-1a therefore creates new avenues to target HIF-1 within a specified disease context. Our study demonstrates that PIM1 inhibition eradicates HIF-1a in JAK2V617F cells, and corrects aberrant lineage committal decisions within JAK2V617F HSPCs. These data therefore present mechanistic insights into the downstream effects of PIM1 inhibition on transcription, which include reversing the pathological activation of HIF-1. Future studies investigating alterations in the phospho/total-proteome in JAK2V617F cells treated with PIM1 inhibitors would bring further value into the modality of action of this therapeutic approach within MPNs.

ChIP-MS/RIME performed on HIF-1a in triple negative breast cancer (Yang *et al.*, 2022) and renal cell carcinoma (Patel *et al.*, 2022) cell lines exposed to hypoxia demonstrated that with a few notable exceptions (e.g. HIF-1B/ARNT and TRIM28), the transcription partners of HIF-a are heavily dictated by the tissue/cancer-context. By applying miniatuRIME to isogenic paired WT JAK2/JAK2V617F haematopoietic progenitor cell lines, our study approach provided a clean genetic system to identify those partners specifically recruited to HIF-1 by JAK2V617F signalling in haematopoietic progenitor cells, as opposed to identifying tissue- or cancer-context associated factors. These findings hold particularly pertinent implications for targeting HIF-1 within haematopoietic malignancies, where eradication of the malignant clone whilst sparing normal haematopoiesis is the gold standard therapeutic approach.

We observed significantly higher HIF-1a protein levels at the chromatin in JAK2V617F cells compared to WT JAK2 cells by mass spectrometry, despite equal HIF-1a protein levels and chromatin input into miniatuRIME assays across experimental conditions. Unexpectedly, this was paired with reduced peak intensity of associated genomic DNA as determined by NGS (ChIP-Seq). STRING analysis of the protein partners of HIF-1a in JAK2V617F cells (normalised against the geometric mean of HIF-1a spectral counts to account for the above increased HIF-1 protein observed in these cells) identified an enrichment of RNA-binding/processing factors including TDP-43, Khdrbs1/Sam68, Fau and Znf638. Taken together, these data suggest that HIF-1 may perform a different role at the chromatin in JAK2V617F mutant HSPCs compared to WT JAK2, one that is more distal to DNA. This may account for a reduced association with DNA, coupled with enhanced interaction with post-transcriptional RNA processing factors. This hypothesis is also supported by the identification that HIF-1 binds to intron/exon regions of target genes, and that VF_Hx HIF-1 target genes are both up- and down-regulated at the transcript level, which both also suggest that HIF-1 is performing a transcript regulatory role beyond canonical transcription initiation in the JAK2V617F context. A subset of transcription factors, historically referred to as “coupling proteins” for their role in mechanically and functionally coupling the steps from transcription to translation, regulate pre-mRNA processing via regulation of elongation rates and pre-mRNA imprinting (binding to nascent RNA) (Auboeuf *et al.*, 2005; Rambout, Dequiedt and Maquat, 2018). Notable examples include the Wilms tumour-suppressor protein (WT1), originally identified as a transcription factor initiating growth and development gene expression profiles, which was subsequently demonstrated to localise to nuclear speckles, bind to RNA and splice factors, and regulate gene-expression via splicing (Davies *et al.*, 1998; van Heyningen Nicholas D Hastie, 2004; Markus *et al.*, 2006; Morrison *et al.*, 2006). In triple negative breast cancer cell lines, HIF-1a can bind to TRIM28/DNA-dependent protein kinase (DNAPK) to release paused RNA Pol II, thereby regulating elongation rate and, it is rational to presume, splicing, although this was not investigated in this study (Yang *et al.*, 2022). Our findings further implicate HIF-1 as adopting pre-mRNA splice-regulatory roles in JAK2V617F HSPCs to produce the observed disease-driving regulon of suppressed and activated genes in MPN disease, however further investigation is required to fully elucidated this non-canonical mechanism of HIF-mediated gene expression.

Meta-analysis of ChIP-seq, RNAseq and MPN patient cohort survival studies identify a set of DNA damage response genes that are deregulated by HIF-1 and significantly associated with overall survival of JAK2V617F MPN patients. JAK2V617F-carrying HSPCs are known to accumulate spontaneous DNA damage compared to healthy counterparts due to replication stress and the burden of metabolic products (Nieborowska-Skorska *et al.*, 2017; Toma *et al.*,

2023, 2024; Karami and Skorski, 2024), and activate the DNA damage response (DDR) (Toma *et al.*, 2023, 2024). Our findings identify that malignant co-option of HIF-1 facilitates in part the enhanced DDR via upregulation of PCNA (nucleotide excision repair), (Sheng *et al.*, 2019), BLM helicase (*BLM*; double-strand break repair by homologous recombination (HR)) (Patel *et al.*, 2017), Aurora Kinase B (*AURKB*; mitotic DNA damage checkpoints) (Ma and Poon, 2020) expression and Tankyrase 1 (*TNKS*, HR) (Nagy *et al.*, 2016), each of which is significantly associated with worsened patient survival. Furthermore, we identify these DDR genes are significantly upregulated in patients undergoing spontaneous leukemic transformation.

Lastly, our study identifies a 13-gene HIF-1 signature comprising the aforementioned pathways, significantly associated with both spontaneous leukaemic transformation and overall survival of JAK2V617F positive MPN patients. To our knowledge, these genes have not previously been implicated in MPN disease pathogenesis and therefore represent both novel pathogenic mechanisms and therapeutic targets.

Through direct experimental analysis of the HIF-1 transcription complex and regulon, our study identifies a hitherto unknown co-option of HIF-1 in JAK2V617F MPNs mediated by aberrant phosphorylation of HIF-1 via PIM1 kinase. We identify that in the setting of MPN, HIF-1 is reprogrammed to perform non-canonical roles as a direct result of oncogene signalling pathways, driving malignant phenotypes and revealing new prognostic signatures for MPNs. These findings also illuminate the value of direct analysis of TF complexes within a disease setting, highlighting the discrepancy between canonical HIF-1 regulons and those induced by oncogenic signalling pathways in the context of JAK2V617F MPNs. These identifications provide evidence that functional delineation of the essential homeostatic roles of HIF-1 within normal physiology from those roles co-opted by malignancy is possible, and identifies tractable handles for this as a therapeutic approach within MPNs. Finally, our study warrants future investigations into the malignant co-option of HIFs and the resultant regulons in the pathogenesis of other haematological and solid cancers.

Methods

Animal models

Animals used in this study were C57BL/6 mice (WT) and Jak/2E/B6 Stella Cre heterozygous and homozygous. All mice were bred and housed under specific pathogen-free conditions at the University of York. All animal procedures were approved by the University of York Animal Welfare and Ethical Review Board and carried out under United Kingdom Home Office license (x). Animals were euthanized by CO2 asphyxia and cervical dislocation. All the mice were 8 to 12 weeks old.

Lineage negative hematopoietic progenitor cell isolation and expansion

Lineage negative cells were isolated from the pelvis, femurs and tibias of C57BL/6 (WT) and Jak/2E/B6 Stella Cre mice using EasySep™ Mouse Hematopoietic Progenitor Cell Isolation Kit (STEMCELL Technologies) according to the manufacturer's protocol. After enrichment cells were plated in expansion culture PVA media and incubated at 5% CO_2 and either 1% O_2 or 21% O_2 (Invivo 500 hypoxic workstation or Binder CO2 incubator) for 6 hours as previously described (Igarashi *et al.*, 2023).

Cell culture

BaF3 cells stably expressing the human MPL and human JAK2 (BaF3 hMPL hJAK2 WT) or the JAK2V617F mutant (BaF3 hMPL hJAK2 VF) were grown in RPMI media (10% FBS, 1% penicillin/streptomycin/L-glutamine) plus murine IL-3. Cells were incubated at 5% CO_2 and the indicated O_2 concentrations.

ChIP

Chromatin immunoprecipitation (ChIP) was performed on BaF3 cells and lineage negative hematopoietic progenitor cells. Cells were incubated at the indicated O_2 concentrations for 6 hours and then fixed with 1% formaldehyde for 10 minutes at room temperature (RT), then neutralised by the addition of 10x Glycine for 5 minutes at RT. The samples were then processed using SimpleChIP® Enzymatic Chromatin IP Kit, Magnetic Beads (Cell Signaling Technology) according to the manufacturer's protocol. ChIP was performed with HIF-1α (D1S7W) XP® Rabbit mAb (Cell Signaling Technology). DNA was isolated using a ChIP DNA Clean & Concentrator (Zymo Research).

Western blot

Cells were cultured at the indicated conditions. Cells were lysed in cell lysis buffer (20 mM Tris-HCl (pH 7.5), 150 mM NaCl, 1 mM Na_2EDTA, 1 mM EGTA, 1% Triton) plus Halt™ Protease and Phosphatase Inhibitor Cocktail, EDTA-free (ThermoFisher Scientific). Lysate (20 µg) was separated on 4-20% Mini-PROTEAN® TGX Stain-Free™ protein gels (Biorad) and transferred onto Immun-Blot® Low Fluorescence PVDF membrane (Biorad). Membranes were probed for the indicated antibodies (see Supplementary Information).

Immunoprecipitation

Cells were cultured at the indicated conditions. Cells were lysed in cell lysis buffer (20 mM Tris-HCl (pH 7.5), 150 mM NaCl, 1 mM Na_2EDTA, 1 mM EGTA, 1% Triton) plus Halt™ Protease and Phosphatase Inhibitor Cocktail, EDTA-free (ThermoFisher Scientific). 200 µg of cell lysate used as input for immunoprecipitation. Cell lysates were precleared by addition

of Protein A magnetic beads (Cell Signaling Technologies) for 20 minutes at RT with rotation followed by magnetic separation. Proteins were captured by addition of HIF-1α (D1S7W) XP® Rabbit mAb (Cell Signaling Technology) and incubated overnight at 4°C with rotation followed by immunoprecipitation by addition of Protein A magnetic beads and incubation for 20 minutes at RT, followed by magnetic separation and washing. Immunoprecipitated protein as then analysed by western blotting.

MiniatuRIME

$5x10^7$ BaF3 hMPL hJAK2 WT or BaF3 hMPL hJAK2 VF cells were incubated at the indicated O_2 concentrations for 6 hours. Cells were fixed by addition of 2mM Disuccinimidyl glutarate (DSG) for 20 minutes with agitation, pelleted by centrifugation at 500xg for 5 minutes RT, and then resuspended into 1% formaldehyde for 10 minutes at room temperature (RT), then neutralised by the addition of 10x Glycine for 5 minutes at RT. Sample processing and immunoprecipitations were performed as described previously (Guertin *et al.*, 2018; Papachristou *et al.*, 2018).

Mass spectrometry

Protein was on-bed digested with trypsin, without reduction or alkylation. Peptides were desalted by C18 ZipTip before drying and resuspending in aqueous 0.1% TFA for LC-MS. Peptides were acquired over a 1 h acquisition with elution from a 50 cm EN PepMap C18 column driven by a Waters mClass UPLC onto an Orbitrap Fusion Tribrid mass spectrometer operated in DDA mode. MS1 spectra were acquired in the Orbitrap mass analyser at 120K resolutions and a cycle time of 1 s, with MS2 spectra acquired in parallel in the linear ion trap using TopSpeed selection. LC-MS chromatograms in .raw format were imported into Progenesis QI for peak picking and chromatographic alignment, before exporting a concatenated tandem mass list in .mgf format for Mascot database searching. Searching was performed against the mouse subset of the SwissProt database appended with common proteomic contaminants. Peptide spectral matches were filtered to 1% FDR using the percolator algorithm and as assessed empirically against a reverse database search. Accepted peptide identifications were imported into Progenesis QI, associated with the chromatographic data and mapped between runs. Data were further filtered to require a minimum of two unique peptides per protein quantification. Relative protein quantification was inferred from peptide precursor ion areas using unique, non-conflicting peptides only and after normalisation to total peptide intensity among runs. Statistical testing between groups was done using anova with the null hypothesis being that proteins are of equal abundance between all samples. The Hochberg and Benjamini FDR methodology was used for multiple test correction of p-values to q-values.

Figure legends:

Figure 1

(A) JVF stabilises HIF-1α independent of oxygen levels in monogenic JVF and JVF MPN immortalised cell lines. Immunoblotting of normoxic cultured wildtype and JVF UT7/TPO and hMPL BaF3 cells, JVF heterozygous SET2 cells and JVF homozygous HEL cells. Immunoblotting carried out using HIF-1α antibody with β actin as a loading control (n=1).

(B) JVF stabilises HIF-1α independent of oxygen levels in primary mouse lineage-Sca1+cKit+ (LSK) cells from JVF homozygous, heterozygous and wildtype C57/BL6 mice. Histogram distribution of fluorescent intensity and cell count from cells probed with FITC-labelled HIF-1α antibody, following ex-vivo culture in hypoxic (blue) or normoxic (purple) conditions (n=1).

(C) Treatment with ROS scavenger NAC fails to inhibit JVF-induced HIF-1α stabilisation. Immunoblotting of wildtype and JVF UT7/TPO cells treated with either NAC, SMI-4a or vehicle control. Immunoblotting carried out using HIF-1α, T389 p70 S6K, p70 S6K and PIM1 antibodies with β actin as a loading control (n=3).

(D)(I) Kinase cascade activity downstream of JAK2 shows significant differences between TPO-stimulated JAK2 and JVF-mediated constitutive signalling. Wildtype and JVF UT7/TPO cells starved or treated with TPO and analysed by multiplex fluorescent barcoding and phospho-flow cytometry. Data normalised by generating a Z score of the mean from 3 independent experiments (±SEM) (n=3).

(II) Proportional representation of total kinase cascade signalling downstream of JAK2 shows an increase in the relative amount of STAT1 and STAT5 activation in JVF cells compared to TPO/MPL stimulation of wildtype JAK2 (n=3).

(E) Database analysis of STAT1 and STAT5 target genes show PIM1 as the sole known kinase of HIF-1α. STAT1 gene targets indicated in purple, STAT5 gene targets indicated in blue, shared STAT1 and STAT5 targets indicated in green, of which are kinases shown in yellow.

(F) PIM1 transcript expression is significantly higher in JVF mouse MEPs compared to wildtype. Bulk RNA-seq analysis of mouse MEPs from wildtype (n=8) and JVF heterozygous mice (n=12).

(G) PIM1 transcript expression is significantly higher in both total and lineage negative mouse bone marrow. qRT-PCR of homozygous JVF and wildtype mouse bone marrow HSPCs (total and lineage negative) with GAPDH as a housekeeping gene control (n=3).

(H) PIM1 transcript levels are elevated and localised to megakaryocyte progenitor (MkP) population in JVF positive MPN patients compared to healthy controls. UMAP scRNAseq plots of control (top row) and myelofibrosis (bottom row) HSPCs with PIM1 transcript highlighted in purple.

Figure 2

(A)(I) Treatment with a variety of PIM1 inhibitors inhibits JVF-mediated HIF-1α stabilisation. Immunoblotting of JVF UT7/TPO cells starved overnight or cultured with TPO and treated with the indicated PIM inhibitor for 6hrs at the indicated dose. Immunoblotting carried out using HIF-1α, HIF-1β, pT389 S6, p70 S6K and PIM1 antibodies with β actin as a loading control (n=3).

(II) Treatment with SMI-4a restores JVF-stabilised HIF-1α levels to wildtype TPO-induced, whilst treatment with Ruxolitinib ablates it. Barcoded phospho-flow cytometry of HIF-1α levels in JVF and wildtype UT7/TPO, cultured in normoxic (20% O_2) or hypoxic (1% O_2) conditions, starved overnight or treated with TPO and treated with SMI-4a, Ruxolitinib or vehicle control. Data normalised by generating a Z score of the mean from 3 independent experiments (±SEM) (n=3).

(B)(I) Treatment with SMI-4a leaves JAK2 signalling cascades untouched whilst treatment with Ruxolitinib ablates them. Immunoblotting of SET2 and HEL cells treated with Ruxolitinib, SMI-4a or vehicle control, using HIF-1α, pY1007/8 JAK2, JAK2, pY705 STAT3, STAT3, pT389 p70 S6K, p70 S6K, pY204/Y187 ERK1/2 and ERK1/2 antibodies and using β actin as a loading control (n=3).

(II) Treatment with SMI-4a leaves JAK2 signalling cascades untouched whilst treatment with Ruxolitinib ablates them. Barcoded phospho-flow cytometry of kinase cascade constituents downstream of JAK2 in JVF and wildtype UT7/TPO, cultured in normoxic (20% O_2) or hypoxic (1% O_2) conditions, starved overnight or treated with TPO and treated with SMI-4a, Ruxolitinib or vehicle control. Data normalised by generating a Z score of the mean from 3 independent experiments (±SEM) (n=3).

(C) PIM1 inhibition rescues JVF heterozygous LSK and progenitor phenotype, returning the LSK/Prog ratios observed in wildtype expansion cultures. *Ex vivo* expansion of long-term HSCs from wildtype and JVF heterozygous mice in the PVA culture system immunophenotyped after 14 days of expansion and expressed as percentage of lineage negative cell population (n=3).

Figure 3

(A)(I) Two novel JVF-exclusive phosphorylation sites identified on HIF-1α (T498 and S500). Phosphoproteomic mass spectrometry analysis of hypoxia-treated JVF and wildtype UT7/TPO cell lysate enriched for phosphoproteins by TiO_2 and enriched for HIF-1α by immunoprecipitation (n=3).

(II) Two novel JVF-exclusive phosphorylation sites identified on HIF-1α (T498 and S500). Volcano plot of phosphosite signal intensity in hypoxic JVF lysate compared to hypoxic WT lysate vs statistical significance (-log10 adj p value).

(B) S500 site is highly evolutionarily conserved across species. Sequence alignment of species as shown.

(C) Novel JVF-exclusive phosphorylation sites (T498 and S500) fall in ODD between canonical HIF-1α hydroxylation sites (P402 and P564). Ribbon diagram (top) and domain diagram (bottom) of HIF-1α, both coloured by domain. Amino acid sites of interest marked in red on both.

(D) Treatment with proteasome-inhibitor MG132 inhibits SMI-4a-mediated destabilisation of JVF-mediated HIF-1α stabilisation. Immunoblotting of JVF and wildtype UT7/TPO cultured in normoxic or hypoxic conditions treated with SMI-4a, MG132 or a combination of the two, using HIF-1α antibody and using β actin as a loading control (n=1).

Figure 4

(A)(I) Diagram of minatuRIME method: wildtype or JVF hMPL BaF3 cells cultured in normoxic (20% O_2) or hypoxic conditions (1% O_2) have their nuclear material crosslinked to retain DNA-bound proteins, fragmented and HIF-1α containing fragments immunoprecipitated by the addition of HIF-1α antibody. The sample is then divided for concurrent analysis by both ChIP-seq (to determine HIF-1αs genomic binding loci) and mass spectrometry (RIME- Rapid immunoprecipitation mass spectrometry of endogenous protein) (to determine HIF-1αs associated transcription cofactors).

(II) JVF causes significantly increased abundance of HIF-1α protein at the DNA yet is significantly less bound to it compared to wildtype. RIME-mass spec analysis of HIF-1α abundance at the chromatin (left) and ChIPseq analysis of the genomic loci bound by HIF-1α (right) in wildtype and JVF hMPL BaF3 cells cultured in either normoxic or hypoxic conditions (n=3).

(B) Whilst several cofactors are found to be common between conditions, a number are identified as unique to JVF in both normoxia and hypoxia. Venn diagram displaying number of cofactors unique to each condition shown as determined by RIME-mass spec.

(C) RIME-mass spec identified HIF-1α cofactors displayed as a heatmap by binding intensity (Log_2FC), normalised to HIF-1α protein levels. Wildtype and JVF hMPL BaF3 cells cultured in either normoxic or hypoxic conditions and subjected to RIME-mass spec (n=3).

(D) Distinct JVF-unique functional protein clusters are enriched in HIF-1α cofactor analysis. STRING analysis was performed on RIME-mass spec protein hits. For each treatment condition, structural and non-mouse proteins were discarded, and RIME hit proteins were sorted by geomean (relative to HIF-1α) and those less than 0.01 discarded. The remaining proteins were then run through the STRING analysis online database and clustered via MCL clustering (stringency 3). Resulting connections plotted by confidence (cutoff 'medium' – 0.04).

(E) Key cofactors were identified as both uniquely up and downregulated in association with HIF-1α. Wildtype and JVF hMPL BaF3 cells cultured in either normoxic or hypoxic conditions and subjected to RIME-mass spec, the top 17 most significantly up or down regulated proteins in both JVF normoxic and hypoxic cells plotted on chart (n=3).

(F)(I) Key cofactors validated by HIF-1α immunoprecipitation. Immunoblotting of HIF-1α-immunoprecipitated wildtype and JVF UT7/TPO cells cultured in either normoxic or hypoxic conditions, treated with or without SMI-4a, with TPO-treated wildtype normoxic cells as a control. Input on left, IP on right. Antibodies for HIF-1α, HIF-1β, TDP-43, Golga3, SIK2 and IMPDH used with β-actin used as loading control (n=2).

(II) TDP-43 JVF-unique cofactor validated by TDP-43 immunoprecipitation of HIF-1α. Immunoblotting of TDP-43-immunoprecipitated wildtype and JVF UT7/TPO cells cultured in either normoxic or hypoxic conditions, with HIF-1α and TDP-43 antibodies used with β-actin used as loading control (n=2).

Figure 5

(A) Diagram of minatuRIME method: wildtype or JVF hMPL BaF3 cells cultured in normoxic (20% O_2) or hypoxic conditions (1% O_2) have their nuclear material crosslinked to retain DNA-bound proteins, fragmented and HIF-1α containing fragments immunoprecipitated by the addition of HIF-1α antibody. The sample is then divided for concurrent analysis by both ChIP-seq (to determine HIF-1αs genomic binding loci) and mass spectrometry (RIME- Rapid immunoprecipitation mass spectrometry of endogenous protein) (to determine HIF-1αs associated transcription cofactors).

(B) Weaker overall binding to genomic loci observed in normoxic and hypoxic JVF cells compared to hypoxic wildtype. ChIPseq analysis of global genomic HIF-1α binding in wildtype and JVF hMPL BaF3s cultured in normoxic (20% O_2) or hypoxic (1% O_2) conditions as displayed by median peak intensity.

(C) Distribution of HIF-1α genomic loci by condition-rank identifies a global redistribution of HIF-1α priority binding in JVF cells. Δrank-score of HIF-1α-bound genomic loci for VF_Nx (left) VF_Hx (right) as determined by ChIPseq.

(D) Chromosomal distribution of HIF-1α site intensity ranking for VF_Nx (light blue) and VF_Hx (dark blue) hMPL BaF3 cells as determined by ChIPseq.

(E) Gene tracks of key significantly bound sites in VF_Hx (green) and VF_Nx (yellow) compared to WT_Hx (blue).

(F) (Upper) Peak intensity at HIF-1 binding loci (ChIPSeq) does not correlate to gene accessibility determined by scATACSeq (Izzo *et al.*, 2024). (Lower) Gene expression (RNAseq) (Li *et al.*, 2022) comparative to gene accessibility.

(G) Proportion of HRE binding

(H) Genomic features of HIF-1 binding sites

Figure 6

(A) Diagram of derivation of 'gene signatures': Top 200 enriched genomic loci from HIF-1α ChIP-seq analysis with q<0.03 for each condition selected for further GSEA analysis.

B)(I) GO/KEGG analysis of WT_Hx 'gene signature' shows canonical HIF-1 pathway association with gene signature data displayed as enrichment bubble plots in ascending order of statistical significance as designated by p-value (from 0.01 to 0.04) with 'bubble' size indicating number of genes associated with the indicated function and as chord plots below.

(I) VF_Nx and (II) VF_Hx 'gene signature' shows significantly altered pathway association

(C) WT_Hx 'gene signature' shows no correlation with disease severity by MIPPS70 (Mutation-Enhanced International Prognostic Score System for transplantation eligible-aged patients with overt PMF) score than wildtype hypoxic gene signature. Data from 230 JAK2V617F mutation positive MPN patients takes into account haemoglobin <10 g/dL (1 point), leukocyte count >25×10^9/L (2 points), platelet count <100×10^9/L (2 points), circulating blasts ≥2% (1 point), MF-2 or higher bone marrow fibrosis grades (1 point), presence of constitutional symptoms (1 point), absence of *CALR* type-1 mutation (1 point), and presence of HMR mutations (*ASXL1, EZH2, SRSF2*, and *IDH1/2*; 1 point for single mutation and 2 points for ≥2 HMR mutated genes) as independent prognostic factors of inferior OS. The MIPSS70 classified the MF patients into three groups: low-risk (0–1 point), intermediate-risk (2–4 points), and high-risk (≥5 points). VF_Nx 'gene signature' shows mild correlation with disease severity. VF_Hx 'gene signature' shows significant correlation with disease severity.

(D) WT_Hx 'gene signature' shows no correlation with JVF MPN patient survival by. VF_Nx 'gene signature' shows mild correlation with poorer survival. VF_Hx 'gene signature' shows significant correlation with poorer survival. Patient survival curve displayed with p values indicating statistical significance of gene signature impacting upon patient survival.

Figure 7

(A) Diagram illustrating derivation of specific genes responsible for differential survival in patients with high VF_Hx signature expression. Genes unique to VF_Hx signature run through scATACseq, bulk mouse RNAseq and scRNAseq human datasets, any genes significantly upregulated in all three run through patient dataset and remaining genes associated with survival examined.

(B) Bulk RNAseq analysis in primary haematopoietic stem and progenitor cells (HSPCs) from jak2$^{wt/wt}$ and jak2$^{vf/vf}$ C57/BL6 mice with VF_Hx HIF-1 gene signatures highlighted in blue. LSKs (top) and MEPs (bottom).

(C)(I) UMAP scRNAseq plots of control (top row) and myelofibrosis (bottom row) HSPCs with transcripts of genes of interest (PCNA, BLM and AURKB) highlighted in purple. Genes of interest correlation with MIPPS70 patient scores displayed below.

(II) MPN patient survival curves with high (red)/low (blue) expression of gene of interest.

(D) UMAP scRNAseq plots of control (top row) and myelofibrosis (bottom row) HSPCs with transcripts of genes of interest (EIF4EBP1) highlighted in purple. Gene of interest correlation with MIPPS70 patient scores and MPN patient survival curves with high (red)/low (blue) expression of gene of interest displayed below.

Figure 8

(A) Full list of genes derived from process described in Fig. 7A displayed by their association with risk of spontaneous AML transformation (top row significant positive correlation with expression, middle row no significant correlation, bottom row significant negative correlation with expression).

(B) (Left to right) Overall disease severity association, myelofibrosis progression, risk of spontaneous AML transformation and survival of patients with high expression of genes from sub-VF_Hx gene signature (top row of Fig. 8).

Supplementary Figures

(S1)(A) Representative intracellular flow cytometry plot for anti-HIF-1a-PE staining in HSC-derived 20%, 5%, or 1% O_2 cultures.

(B) Mean frequency of $CD201^+CD150^+$KSL cells (left), mean number of live cells per well (middle), and mean frequency of $Lineage^+$ cells (right) within 10-day HSC-derived cultures at 20% O_2, 5% O_2, or 1% O_2, cultured with either DMSO or the HIF-1α-specific transcription inhibitor GN44028 (100 nM). n=10. Replating efficiency from cultures described.

(S2)(A) Violin plot of flow cytometry data from Fig. 1B normalised to isotype.

(B) Western blot of primary mouse HSCs from wildtype, heterozygous and homozygous JVF mice treated with the displayed length of hypoxia and quantification by densitometry.

(S3)(A) *Ex vivo* expansion of long-term HSCs from wildtype and JVF heterozygous mice in the PVA culture system immunophenotyped after 14 days of expansion and expressed as percentage of lineage negative cell population (n=3). Treated with indicated dose of HIF-1 inhibitor GN44028 and proportion of LSK population displayed.

(B) *Ex vivo* expansion of long-term HSCs from wildtype and JVF heterozygous mice in the PVA culture system immunophenotyped after 14 days of expansion and expressed as percentage of lineage negative cell population (n=3). Treated with indicated dose of HIF-1 inhibitor GN44028 and proportion of progenitor population displayed.

(S4)(A) repeats of Fig. 1C in SET2 and HEL cell lines.

(B) Repeats of Fig. 1C with the addition of DMF treatment in UT7/TPO JVF and wildtype, SET2 and HEL cells.

(S5) Immunoblotting of JVF UT7/TPO cells treated with ERK inhibitor SCH874 at indicated dose, blotted for pJAK2 Y1007/Y1008, HIF-1α, pERK1/2, ERK1/2 with B-actin as loading control.

(S6) Immunoblotting of HEL cells treated with a variety of STAT inhibitors at doses indicated.

(S7) PIM1 transcript expression is higher in JVF mouse MEPs compared to wildtype. Bulk RNA-seq analysis of mouse LSKs from wildtype and JVF heterozygous mice.

(S8) Gating strategy for multiplex fluorescent barcoding and phospho-flow cytometry.

(S9)(A) Repeat of Fig. 2A(I) in wildtype UT7/TPO cells.

(B) Repeat of Fig. S9A in wildtype and JVF hMPL BaF3 cells

(S11) Full panel of kinase cascade constituents from Fig. 2B(II).

(S12) HSC gating strategy for immunophenotyping of expansion cultures.

(S13) Exemplary plots of HSC immunophenotyping.

(S14) Effect of HIF2a inhibition on expansion culture phenotypes.

(S15) Immunoblot of wildtype and JVF UT7/TPO cells cultured in normoxia or hypoxia and treated with PIM1 inhibitor SMI-4a or ERK inhibitor UO126, blotted for HIF-1a and pHIF1a T455 with b actin as loading control.

(S16)(A) Full STRING functional cluster analysis of all cofactor proteins identified by RIME-mass spec.

(B) STRING functional cluster analysis of cofactors de-enriched for VF_Hx HIF-1a (left) and VF_Nx HIF-1a (right).

(S17) Full panel of phosphorylated proteins identified by phospho mass spec as immunoprecipitated with HIF1a in JVF and wildtype hypoxic UT7/TPO cells.

(S18) Analysis of WT_Hx cells shows canonical HIF signature gene loci binding as determined by ChIPseq in hMPL BaF3 cells.

(S19) Gene tracks of key canonical HIF-signature loci significantly bound in WT_Hx cells in hMPL BaF3 cells.

(S20) Overall mean peak intensity of HIF1a loci binding in the indicated conditions as determined by ChIPseq in hMPL BaF3 cells.

(S21) Venn diagram of HIF1a loci bound in the indicated conditions with number of genes unique to each condition labelled as determined by ChIPseq in hMPL BaF3 cells.

(S22) Genomic distribution of HIF1a binding in VF_Nx and VF_Hx vs WT_Hx as determined by ChIPseq in hMPL BaF3 cells.

(S23) GOTCHA analysis of RNAseq gene expression vs ATACseq gene accessibility.

(S24) Genes from canonical HIF-1 metagene signature identified in VF_Nx and VF_Hx datasets.

(S25) Expression of key JVF-associated genes from bulk RNA-seq analysis of mouse MEP and LSKs.

(S26) UMAP scRNAseq plots of control (top row) and myelofibrosis (bottom row) HSPCs with transcripts of genes of interest (BCL2L1) highlighted in purple. Gene of interest correlation with MIPPS70 patient scores and MPN patient survival curves with high (red)/low (blue) expression of gene of interest displayed below.

(S27) UMAP scRNAseq plots of control (top row) and myelofibrosis (bottom row) HSPCs with transcripts of genes of interest (TNKS, HECTD1, WIPF1, PPID) highlighted in purple. Gene of interest correlation with MIPPS70 patient scores and MPN patient survival curves with high (red)/low (blue) expression of gene of interest displayed below.

(S28) UMAP scRNAseq plots of control (top row) and myelofibrosis (bottom row) HSPCs with transcripts of genes of interest (IER3) highlighted in purple. Gene of interest correlation with MIPPS70 patient scores and MPN patient survival curves with high (red)/low (blue) expression of gene of interest displayed below.

(S29) Full VF_Hx signature association with spontaneous AML transformation.

(S30) Graphical abstract.

References

Auboeuf, D. *et al.* (2005) "A subset of nuclear receptor coregulators act as coupling proteins during synthesis and maturation of RNA transcripts," *Molecular and cellular biology*, 25(13), pp. 5307–5316.

Batie, M. *et al.* (2019) "Hypoxia induces rapid changes to histone methylation and reprograms chromatin," *Science*, 363(6432), pp. 1222–1226.

Baumeister, J. *et al.* (2020) "Hypoxia-inducible factor 1 (HIF-1) is a new therapeutic target in JAK2V617F-positive myeloproliferative neoplasms," *Leukemia*, 34(4), pp. 1062–1074.

Casillas, A. L. *et al.* (2021) "Direct phosphorylation and stabilization of HIF-1α by PIM1 kinase drives angiogenesis in solid tumors," *Oncogene*, 40(32), pp. 5142–5152.

Center for Drug Evaluation and Research (2023) *FDA approves belzutifan for advanced renal cell carcinoma*, *U.S. Food and Drug Administration*. FDA. Available at: https://www.fda.gov/drugs/resources-information-approved-drugs/fda-approves-belzutifan-advanced-renal-cell-carcinoma (Accessed: June 21, 2024).

Davies, R. C. *et al.* (1998) "WT1 interacts with the splicing factor U2AF65 in an isoform-dependent manner and can be incorporated into spliceosomes," *Genes & development*, 12(20), pp. 3217–3225.

Dinarello, A. *et al.* (2023) "STAT3 and HIF1α cooperatively mediate the transcriptional and physiological responses to hypoxia," *Cell death discovery*, 9(1), p. 226.

Dunbar, A. J., Rampal, R. K. and Levine, R. (2020) "Leukemia secondary to myeloproliferative neoplasms," *Blood*, 136(1), pp. 61–70.

Dutta, A. *et al.* (2022) "Genetic ablation of Pim1 or pharmacologic inhibition with TP-3654 ameliorates myelofibrosis in murine models," *Leukemia*, 36(3), pp. 746–759.

Guertin, M. J. *et al.* (2018) "Parallel factor ChIP provides essential internal control for quantitative differential ChIP-seq," *Nucleic acids research*, 46(12), p. e75.

van Heyningen Nicholas D Hastie, S. H. L. J.-P. C. K. M. D. E. M. R. A. R. F. C. V. (2004) "Subnuclear localization of WT1 in splicing or transcription factor domains is regulated by alternative splicing," *Cell*, 81(3), pp. 391–401.

Igarashi, K. J. *et al.* (2023) "Physioxia improves the selectivity of hematopoietic stem cell expansion cultures," *Blood advances*, 7(14), pp. 3366–3377.

Izzo, F. *et al.* (2024) "Mapping genotypes to chromatin accessibility profiles in single cells," *Nature*, 629(8014), pp. 1149–1157.

Karami, A. and Skorski, T. (2024) "DNA damage response genes as biomarkers of therapeutic outcomes in acute myeloid leukemia patients," *Leukemia*, 38(6), pp. 1407–1410.

Keith, B., Johnson, R. S. and Simon, M. C. (2011) "HIF1α and HIF2α: sibling rivalry in hypoxic tumour growth and progression," *Nature reviews. Cancer*, 12(1), pp. 9–22.

Lawson, H. *et al.* (2024) "The selective prolyl hydroxylase inhibitor IOX5 stabilizes HIF-1α and compromises development and progression of acute myeloid leukemia," *Nature cancer*. doi: 10.1038/s43018-024-00761-w.

Li, B. *et al.* (2022) “BMP2/SMAD pathway activation in JAK2/p53-mutant megakaryocyte/erythroid progenitors promotes leukemic transformation,” *Blood*, 139(25), pp. 3630–3646.

Li, J. *et al.* (2014) “JAK2V617F homozygosity drives a phenotypic switch in myeloproliferative neoplasms, but is insufficient to sustain disease,” *Blood*, 123(20), pp. 3139–3151.

Lombardi, O. *et al.* (2022) “Pan-cancer analysis of tissue and single-cell HIF-pathway activation using a conserved gene signature,” *Cell reports*, 41(7), p. 111652.

Ma, H. T. and Poon, R. Y. C. (2020) “Aurora kinases and DNA damage response,” *Mutation research*, 821, p. 111716.

Malkov, M. I., Lee, C. T. and Taylor, C. T. (2021) “Regulation of the Hypoxia-Inducible Factor (HIF) by Pro-Inflammatory Cytokines,” *Cells* , 10(9). doi: 10.3390/cells10092340.

Markus, M. A. *et al.* (2006) “WT1 interacts with the splicing protein RBM4 and regulates its ability to modulate alternative splicing in vivo,” *Experimental cell research*, 312(17), pp. 3379–3388.

Mazzacurati, L. *et al.* (2015) “The PIM inhibitor AZD1208 synergizes with ruxolitinib to induce apoptosis of ruxolitinib sensitive and resistant JAK2-V617F-driven cells and inhibit colony formation of primary MPN cells,” *Oncotarget*, 6(37), pp. 40141–40157.

Mondello, P., Cuzzocrea, S. and Mian, M. (2014) “Pim kinases in hematological malignancies: where are we now and where are we going?,” *Journal of hematology & oncology*, 7, p. 95.

Morrison, A. A. *et al.* (2006) “The Wilms tumour suppressor protein WT1 (+KTS isoform) binds alpha-actinin 1 mRNA via its zinc-finger domain,” *Biochemistry and cell biology = Biochimie et biologie cellulaire*, 84(5), pp. 789–798.

Nagy, Z. *et al.* (2016) “Tankyrases Promote Homologous Recombination and Check Point Activation in Response to DSBs,” *PLoS genetics*, 12(2), p. e1005791.

Nieborowska-Skorska, M. *et al.* (2017) “Ruxolitinib-induced defects in DNA repair cause sensitivity to PARP inhibitors in myeloproliferative neoplasms,” *Blood*, 130(26), pp. 2848–2859.

Ortmann, B. M. (2024) “Hypoxia-inducible factor in cancer: from pathway regulation to therapeutic opportunity,” *BMJ Oncology*. BMJ Publishing Group Ltd, 3(1). doi: 10.1136/bmjonc-2023-000154.

Papachristou, E. K. *et al.* (2018) “A quantitative mass spectrometry-based approach to monitor the dynamics of endogenous chromatin-associated protein complexes,” *Nature communications*, 9(1), p. 2311.

Patel, D. S. *et al.* (2017) “BLM helicase regulates DNA repair by counteracting RAD51 loading at DNA double-strand break sites,” *The Journal of cell biology*, 216(11), pp. 3521–3534.

Patel, S. A. *et al.* (2022) “The renal lineage factor PAX8 controls oncogenic signalling in kidney cancer,” *Nature*, 606(7916), pp. 999–1006.

Pawlus, M. R., Wang, L. and Hu, C.-J. (2014) “STAT3 and HIF1α cooperatively activate HIF1 target genes in MDA-MB-231 and RCC4 cells,” *Oncogene*, 33(13), pp. 1670–1679.

Psaila, B. *et al.* (2020) “Single-Cell Analyses Reveal Megakaryocyte-Biased Hematopoiesis in Myelofibrosis and Identify Mutant Clone-Specific Targets,” *Molecular cell*, 78(3), pp. 477-492.e8.

Rambout, X., Dequiedt, F. and Maquat, L. E. (2018) “Beyond Transcription: Roles of Transcription Factors in Pre-mRNA Splicing,” *Chemical reviews*, 118(8), pp. 4339–4364.

Sheng, C. *et al.* (2019) “PCNA-Mediated Degradation of p21 Coordinates the DNA Damage Response and Cell Cycle Regulation in Individual Cells,” *Cell reports*, 27(1), pp. 48-58.e7.

Toma, M. *et al.* (2023) “Clonal Targeting of DNA Damage Response Pathways Eradicates Myeloproliferative Neoplasms,” *Blood*. American Society of Hematology, 142(Supplement 1), pp. 120–120.

Toma, M. M. *et al.* (2024) “Clonal medicine targeting DNA damage response eradicates leukemia,” *Leukemia*, 38(3), pp. 671–675.

Tsutsumi, N. *et al.* (2023) “Structure of the thrombopoietin-MPL receptor complex is a blueprint for biasing hematopoiesis,” *Cell*, 186(19), pp. 4189-4203.e22.

Wilkinson, A. C. *et al.* (2019) “Long-term ex vivo haematopoietic-stem-cell expansion allows nonconditioned transplantation,” *Nature*, 571(7763), pp. 117–121.

Wilmes, S. *et al.* (2020) “Mechanism of homodimeric cytokine receptor activation and dysregulation by oncogenic mutations,” *Science*, 367(6478), pp. 643–652.

Yan, D., Hutchison, R. E. and Mohi, G. (2012) “Critical requirement for Stat5 in a mouse model of polycythemia vera,” *Blood*, 119(15), pp. 3539–3549.

Yang, Y. *et al.* (2022) “HIF-1 Interacts with TRIM28 and DNA-PK to release paused RNA polymerase II and activate target gene transcription in response to hypoxia,” *Nature communications*, 13(1), p. 316.

Fig. 1

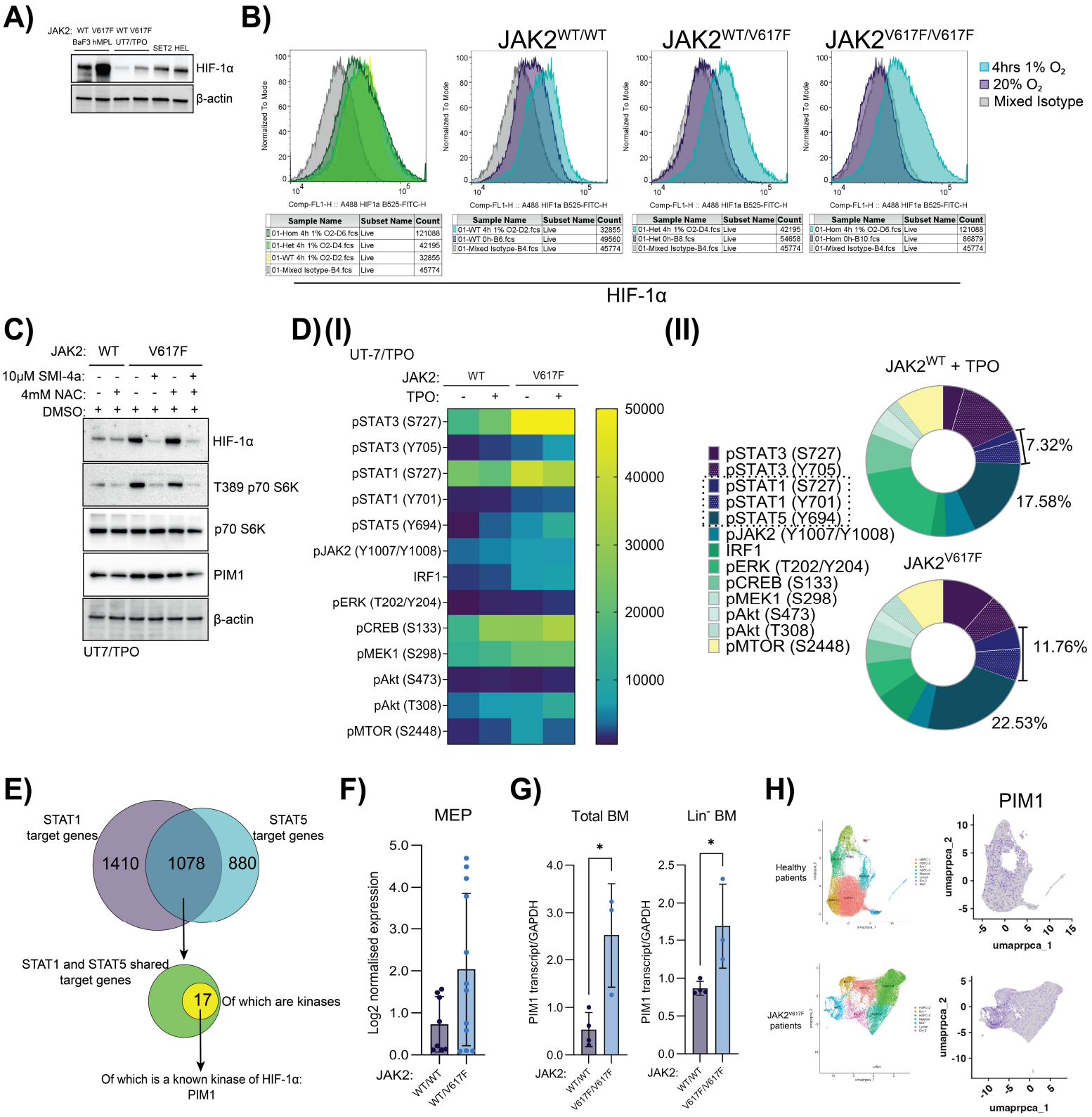
A)
JAK2: WT V617F WT V617F
BaF3 hMPL UT7/TPO SET2 HEL
HIF-1α
β-actin
B)
JAK2WT/WT
JAK2WT/V617F
JAK2V617F/V617F
4hrs 1% O2
20% O2
Mixed Isotype
Normalized To Mode
Comp-FL1-H :: A488 HIF1a B525-FITC-H
HIF-1α
C)
JAK2: WT V617F
10μM SMI-4a:
4mM NAC:
DMSO:
HIF-1α
T389 p70 S6K
p70 S6K
PIM1
β-actin
UT7/TPO
D) (I)
UT-7/TPO
JAK2: WT V617F
TPO:
pSTAT3 (S727)
pSTAT3 (Y705)
pSTAT1 (S727)
pSTAT1 (Y701)
pSTAT5 (Y694)
pJAK2 (Y1007/Y1008)
IRF1
pERK (T202/Y204)
pCREB (S133)
pMEK1 (S298)
pAkt (S473)
pAkt (T308)
pMTOR (S2448)
50000
40000
30000
20000
10000
(II)
JAK2WT + TPO
7.32%
17.58%
JAK2V617F
11.76%
22.53%
E)
STAT1 target genes
STAT5 target genes
1410
1078
880
STAT1 and STAT5 shared target genes
17
Of which are kinases
Of which is a known kinase of HIF-1α: PIM1
F)
MEP
Log2 normalised expression
JAK2: WT/WT WT/V617F
G)
Total BM
Lin- BM
PIM1 transcript/GAPDH
JAK2: WT/WT V617F/V617F
H)
PIM1
Healthy patients
JAK2V617F patients
umaprpca_1
umaprpca_2

Fig. 2

A) (I)

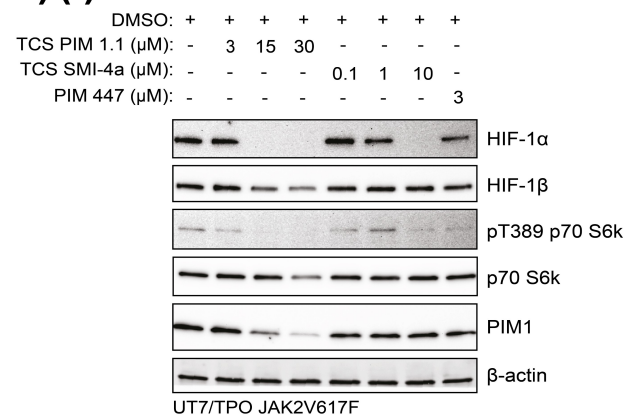

(II)

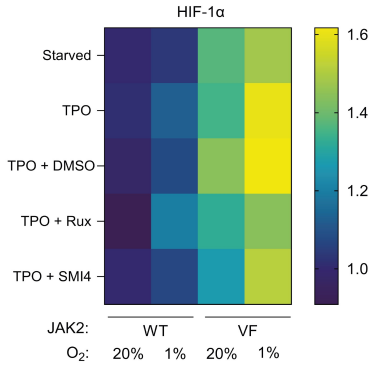

B) (I)

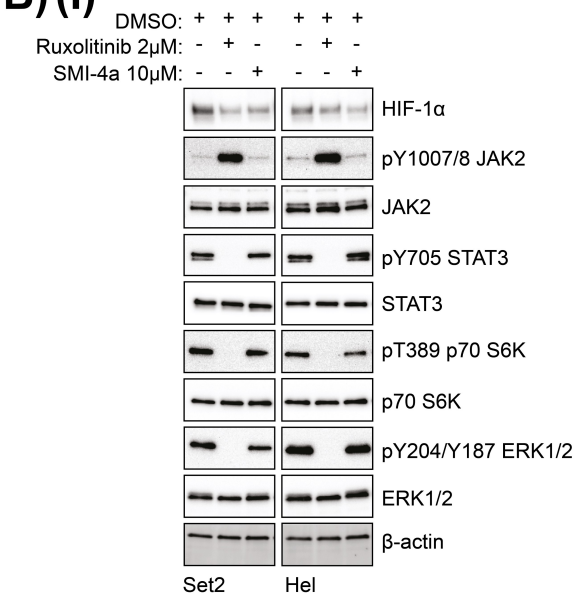

(II)

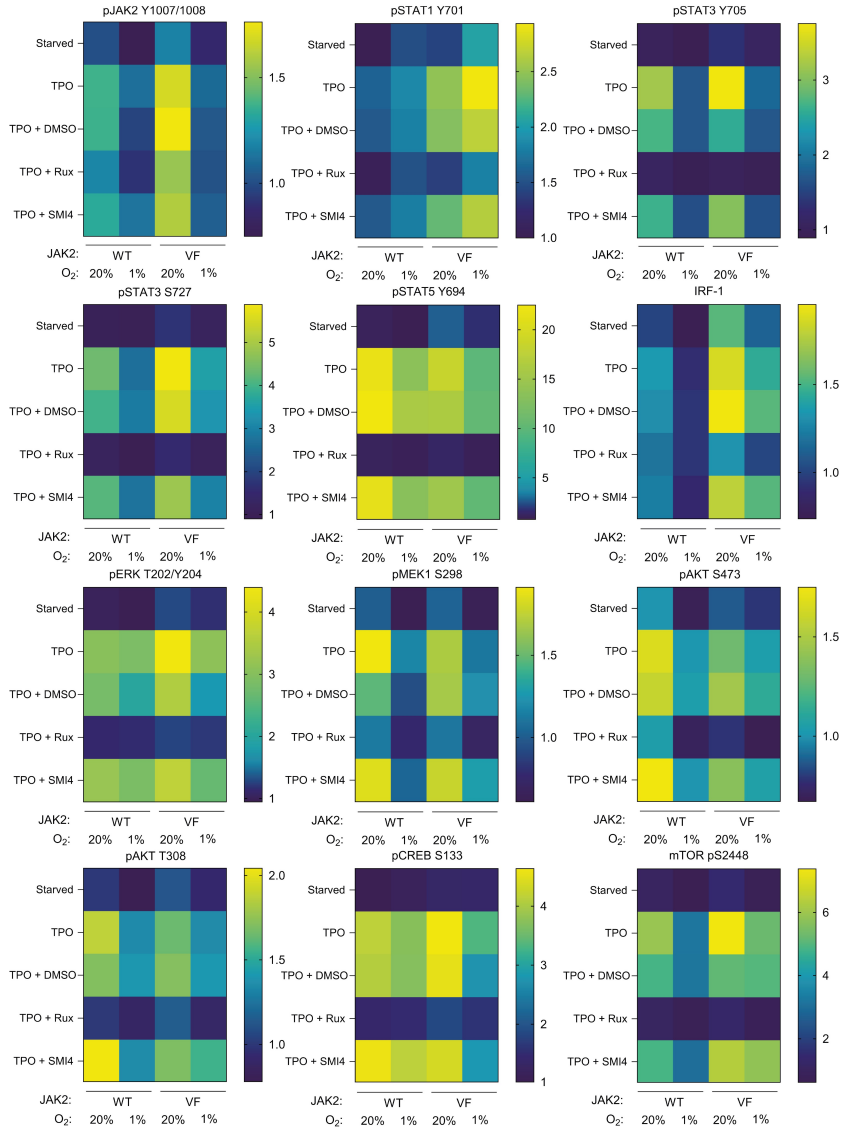

C)

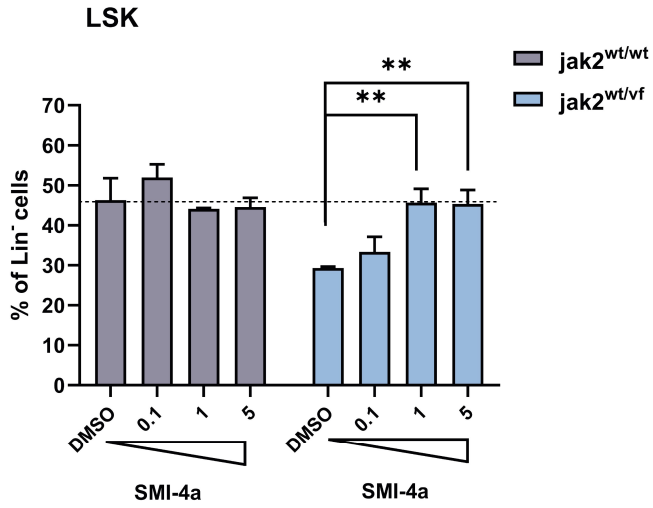

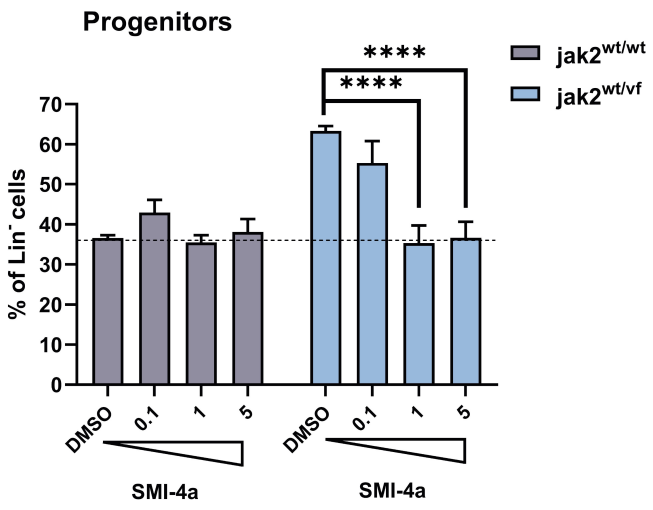

Fig. 3

A) (I)

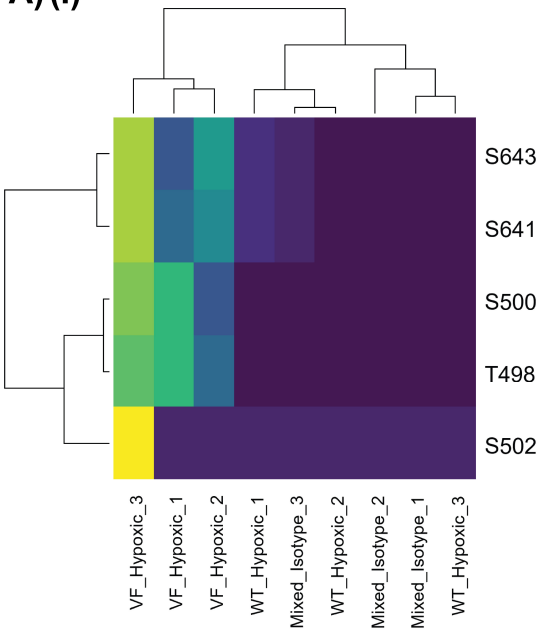

(II)

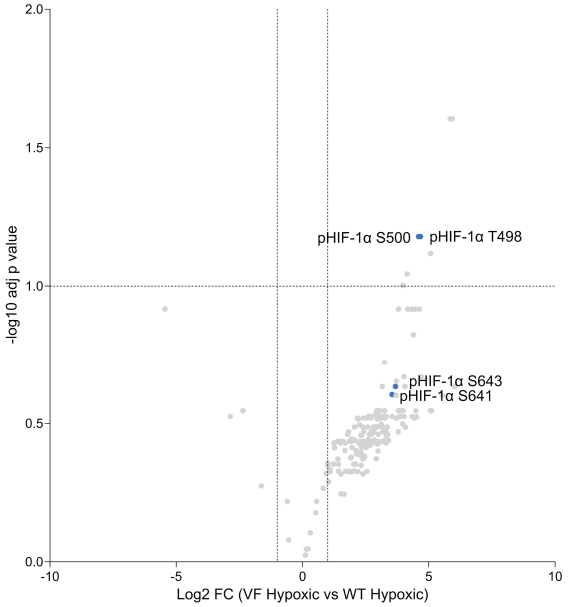

B)

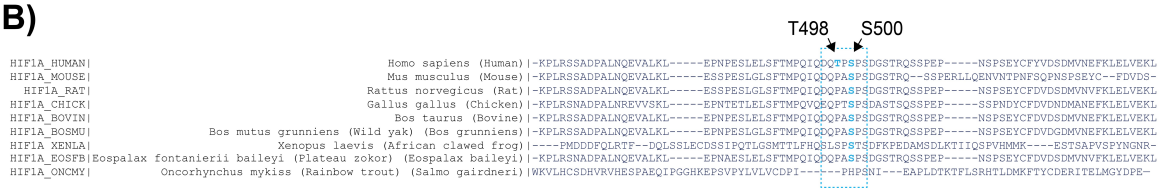

C)

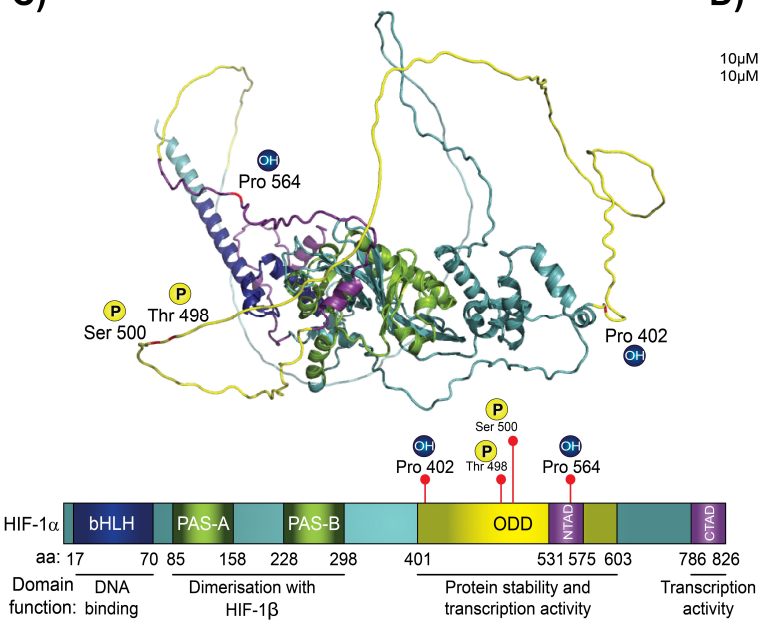

D)

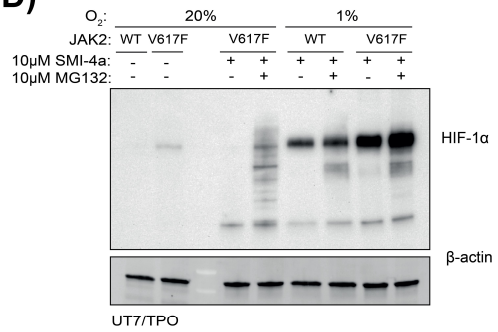

Fig. 4

A)(I)

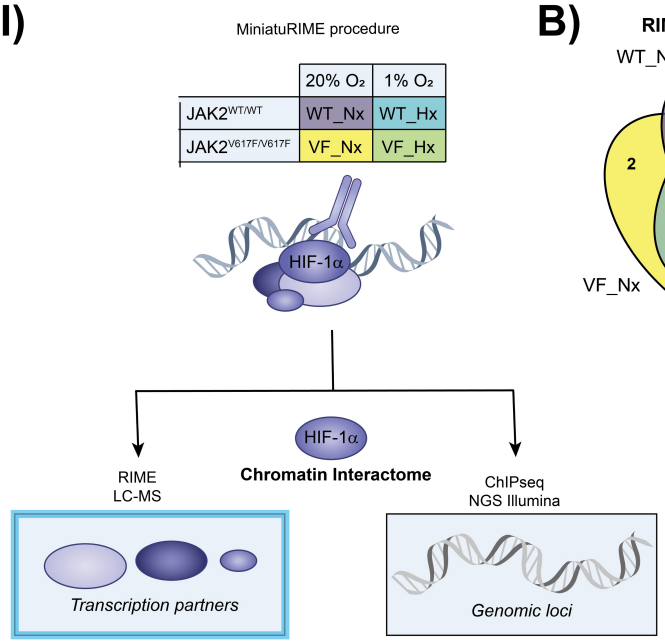

B)

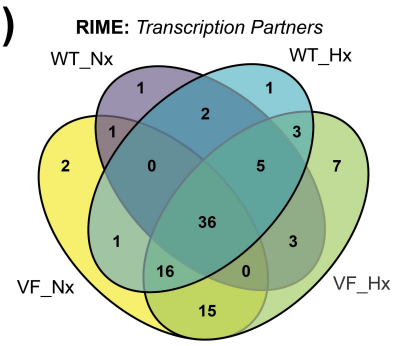

C)

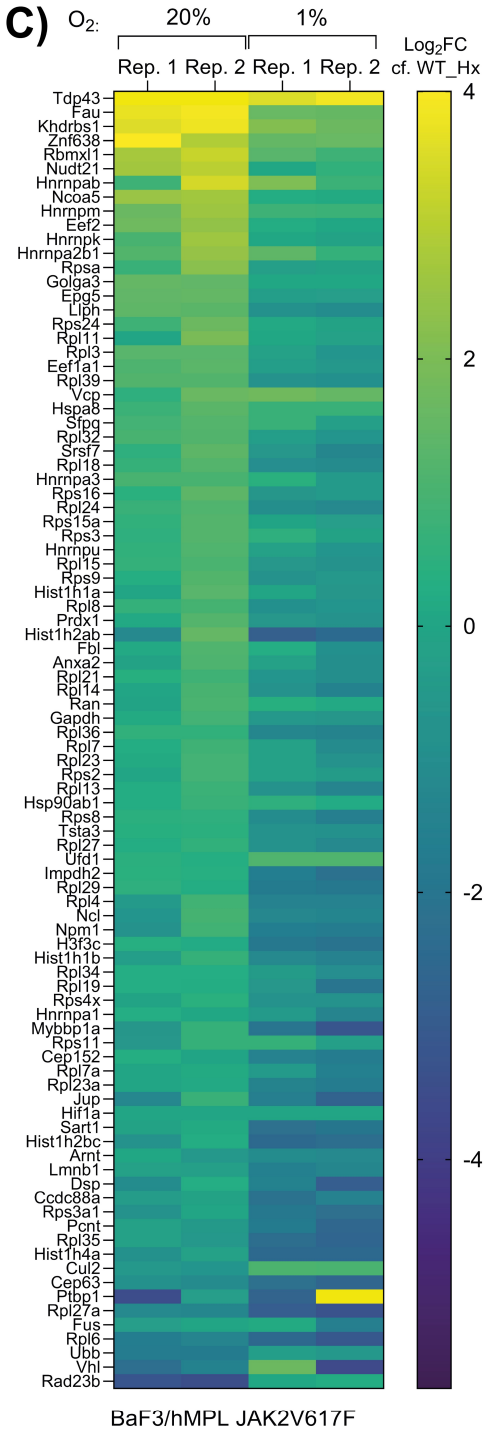

(II)

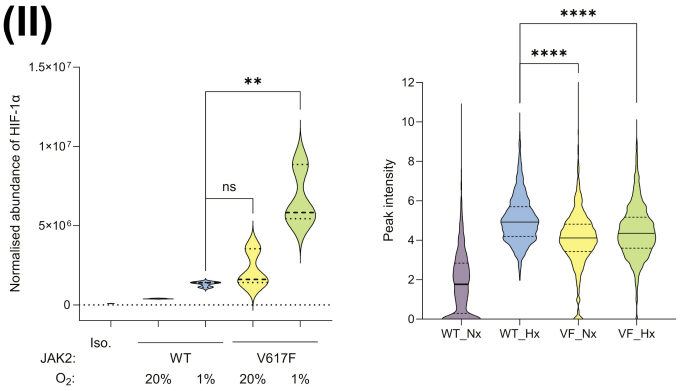

D)

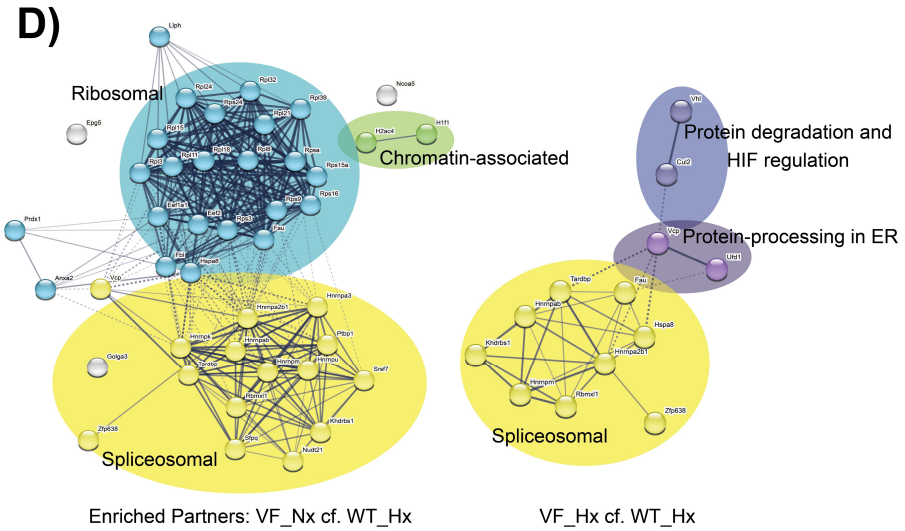

E)

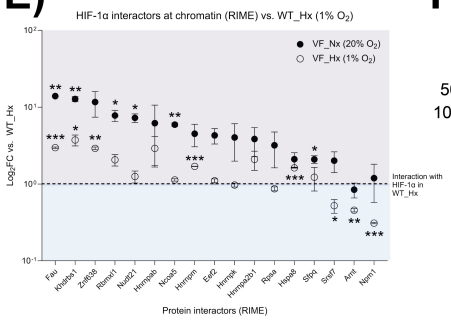

F(I)

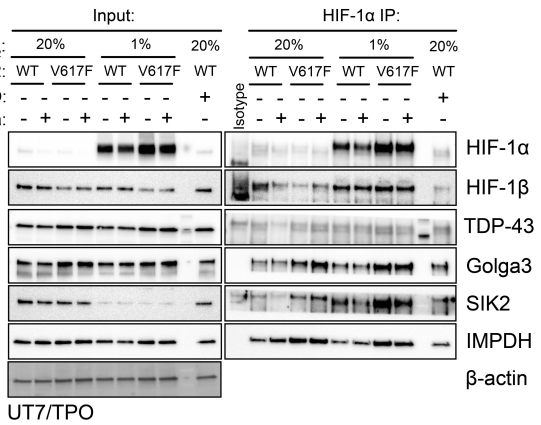

(II)

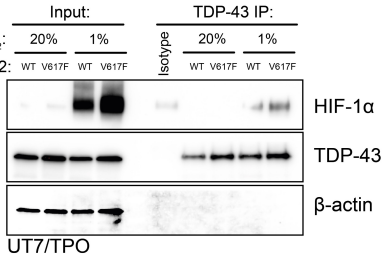

Fig. 5

A)

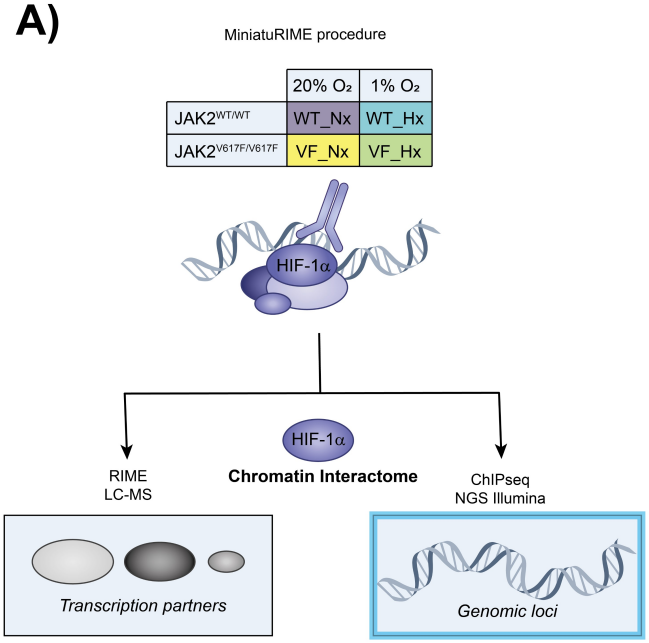

B)

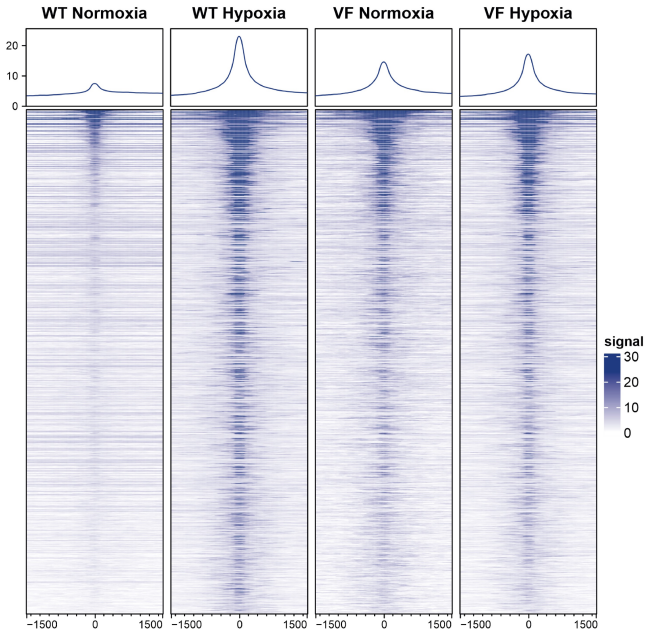

C)

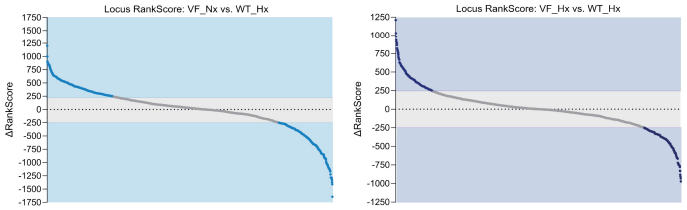

D)

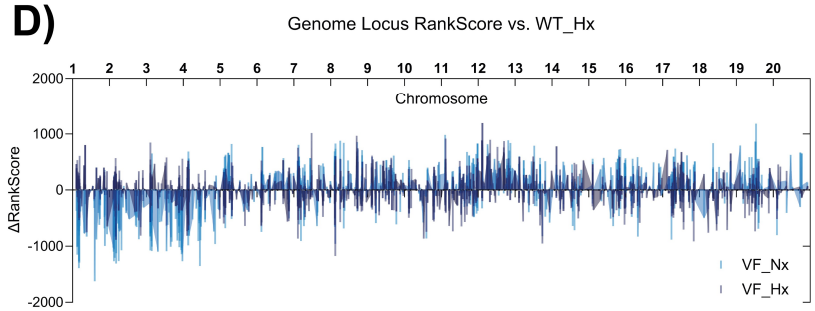

E)

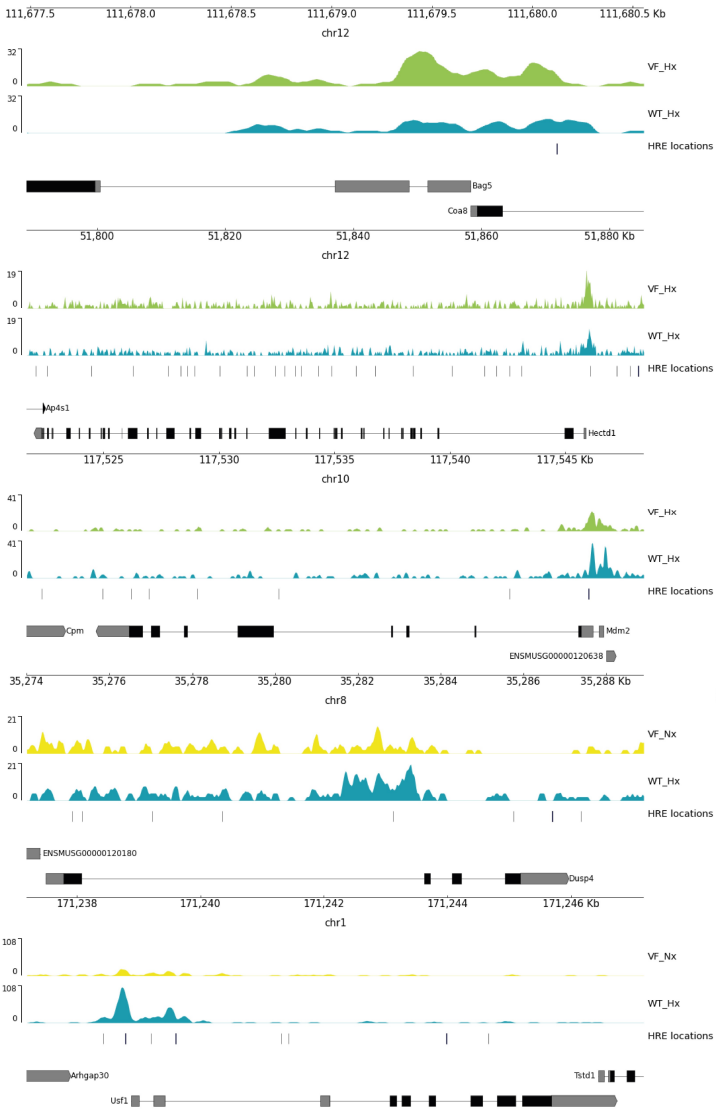

F)

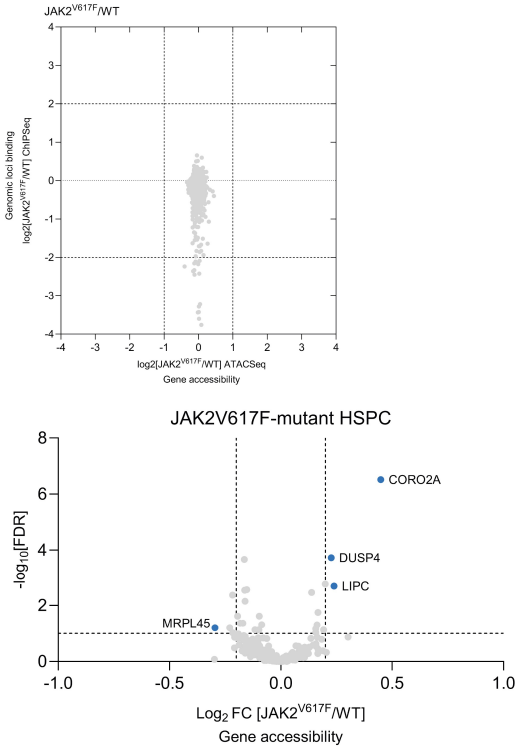

G)

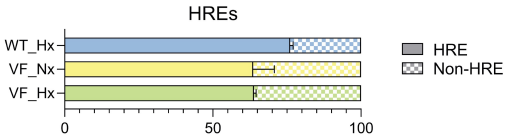

H)

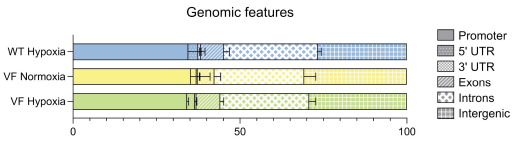

Fig. 6

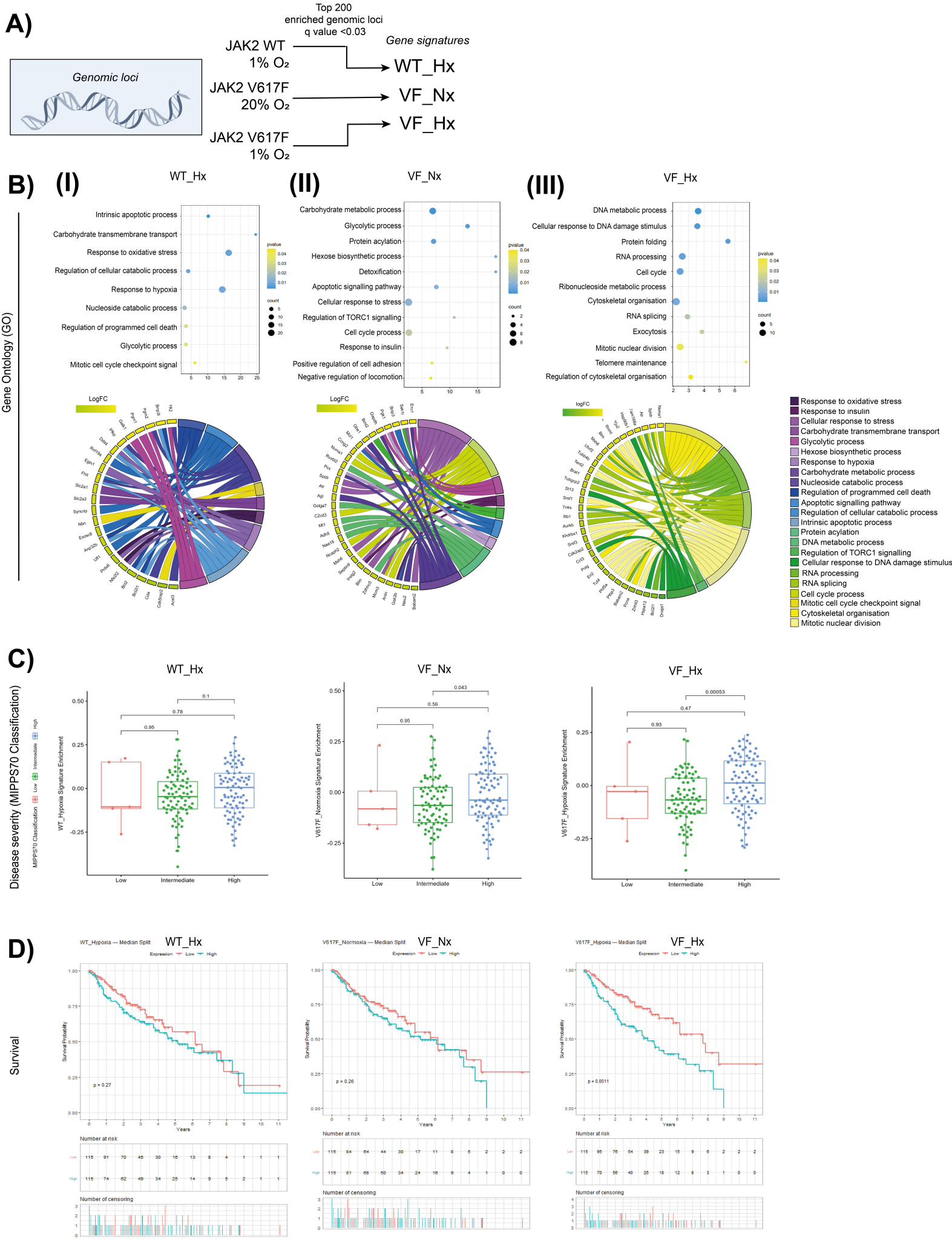
A)
Genomic loci
Top 200
enriched genomic loci
q value <0.03
Gene signatures
JAK2 WT
1% O₂
WT_Hx
JAK2 V617F
20% O₂
VF_Nx
JAK2 V617F
1% O₂
VF_Hx
B)
Gene Ontology (GO)
(I)
WT_Hx
Intrinsic apoptotic process
Carbohydrate transmembrane transport
Response to oxidative stress
Regulation of cellular catabolic process
Response to hypoxia
Nucleoside catabolic process
Regulation of programmed cell death
Glycolytic process
Mitotic cell cycle checkpoint signal
(II)
VF_Nx
Carbohydrate metabolic process
Glycolytic process
Protein acylation
Hexose biosynthetic process
Detoxification
Apoptotic signalling pathway
Cellular response to stress
Regulation of TORC1 signalling
Cell cycle process
Response to insulin
Positive regulation of cell adhesion
Negative regulation of locomotion
(III)
VF_Hx
DNA metabolic process
Cellular response to DNA damage stimulus
Protein folding
RNA processing
Cell cycle
Ribonucleoside metabolic process
Cytoskeletal organisation
RNA splicing
Exocytosis
Mitotic nuclear division
Telomere maintenance
Regulation of cytoskeletal organisation
pvalue
count
LogFC
Response to oxidative stress
Response to insulin
Cellular response to stress
Carbohydrate transmembrane transport
Glycolytic process
Hexose biosynthetic process
Response to hypoxia
Carbohydrate metabolic process
Nucleoside catabolic process
Regulation of programmed cell death
Apoptotic signalling pathway
Regulation of cellular catabolic process
Intrinsic apoptotic process
Protein acylation
DNA metabolic process
Regulation of TORC1 signalling
Cellular response to DNA damage stimulus
RNA processing
RNA splicing
Cell cycle process
Mitotic cell cycle checkpoint signal
Cytoskeletal organisation
Mitotic nuclear division
C)
Disease severity (MIPPS70 Classification)
MIPPS70 Classification
Low
Intermediate
High
WT_Hx
WT_Hypoxia Signature Enrichment
0.95
0.78
0.1
VF_Nx
V617F_Normoxia Signature Enrichment
0.95
0.56
0.043
VF_Hx
V617F_Hypoxia Signature Enrichment
0.93
0.47
0.00053
D)
Survival
WT_Hx
WT_Hypoxia — Median Split
p = 0.27
VF_Nx
V617F_Normoxia — Median Split
p = 0.26
VF_Hx
V617F_Hypoxia — Median Split
p = 0.0011
Expression
Low
High
Survival Probability
Years
Number at risk
Number of censoring

Fig. 7

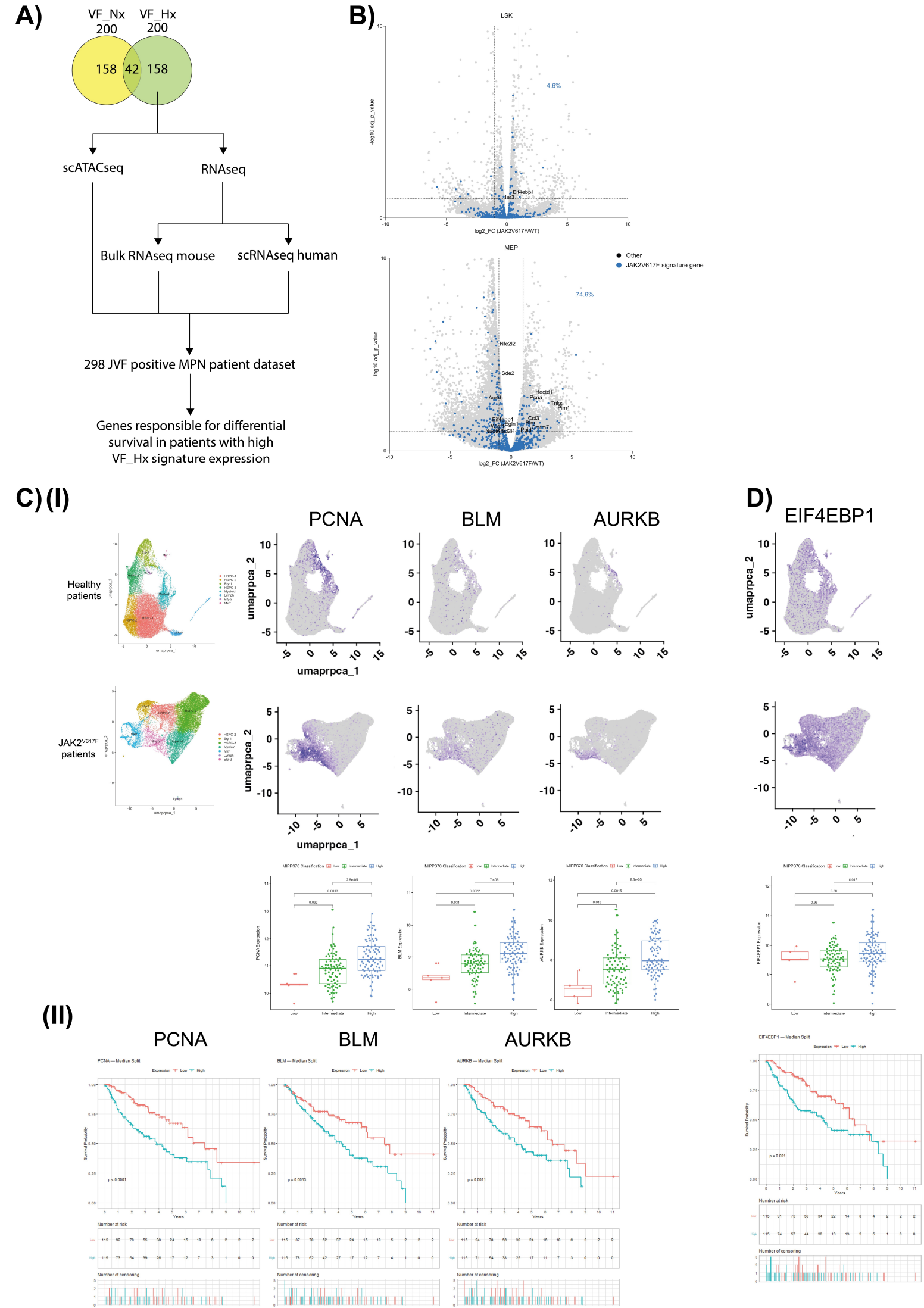
A)
VF_Nx
200
VF_Hx
200
158
42
158
scATACseq
RNAseq
Bulk RNAseq mouse
scRNAseq human
298 JVF positive MPN patient dataset
Genes responsible for differential survival in patients with high VF_Hx signature expression
B)
LSK
4.6%
-log10 adj_p_value
log2_FC (JAK2V617F/WT)
MEP
74.6%
Other
JAK2V617F signature gene
C) (I)
PCNA
BLM
AURKB
D)
EIF4EBP1
Healthy patients
JAK2V617F patients
umaprpca_1
umaprpca_2
(II)
PCNA
BLM
AURKB
PCNA — Median Split
BLM — Median Split
AURKB — Median Split
EIF4EBP1 — Median Split
Number at risk
Number of censoring

Fig. 8

A)

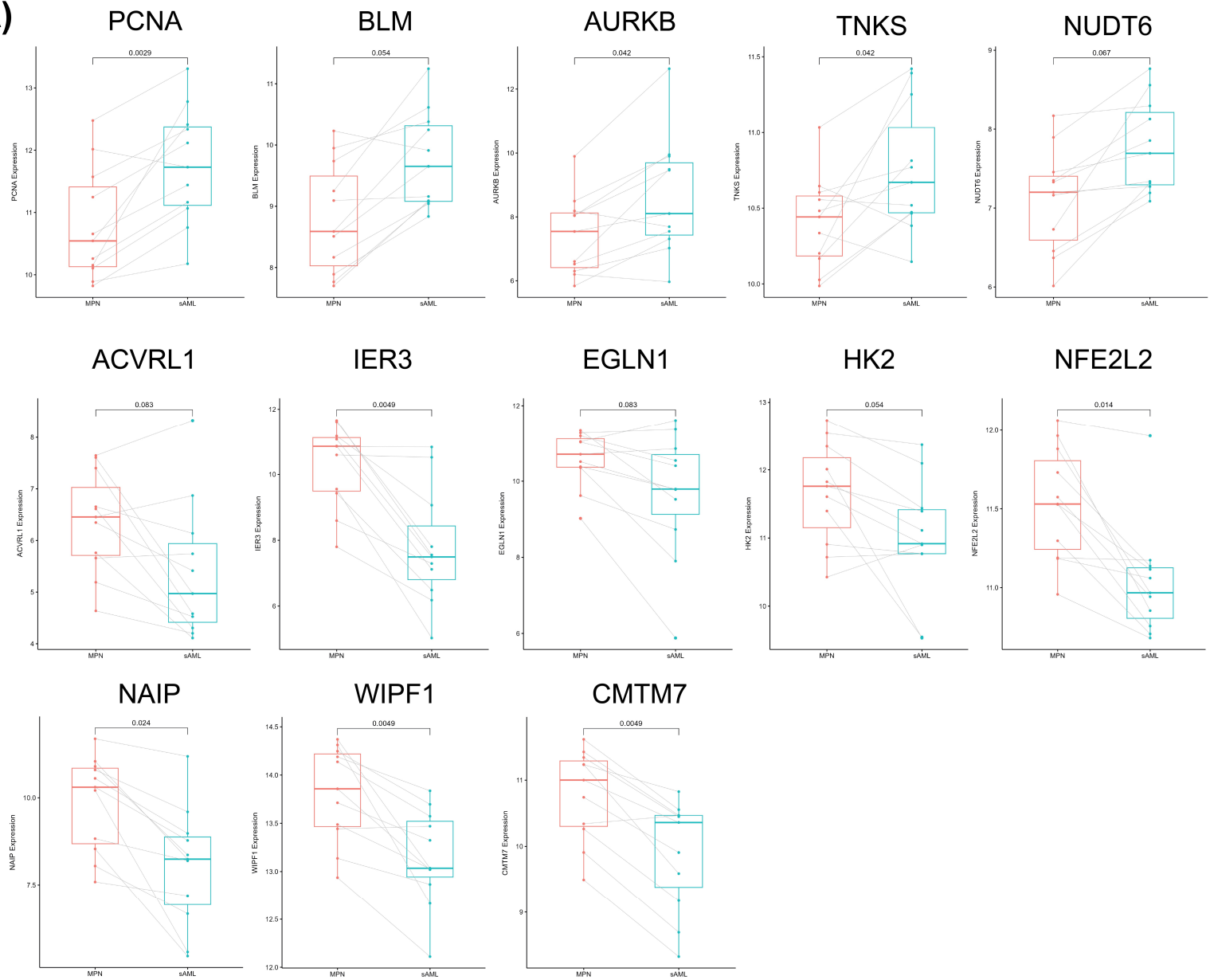
PCNA
0.0029
PCNA Expression
BLM
0.054
BLM Expression
AURKB
0.042
AURKB Expression
TNKS
0.042
TNKS Expression
NUDT6
0.067
NUDT6 Expression
ACVRL1
0.083
ACVRL1 Expression
IER3
0.0049
IER3 Expression
EGLN1
0.083
EGLN1 Expression
HK2
0.054
HK2 Expression
NFE2L2
0.014
NFE2L2 Expression
NAIP
0.024
NAIP Expression
WIPF1
0.0049
WIPF1 Expression
CMTM7
0.0049
CMTM7 Expression
MPN
sAML

B)

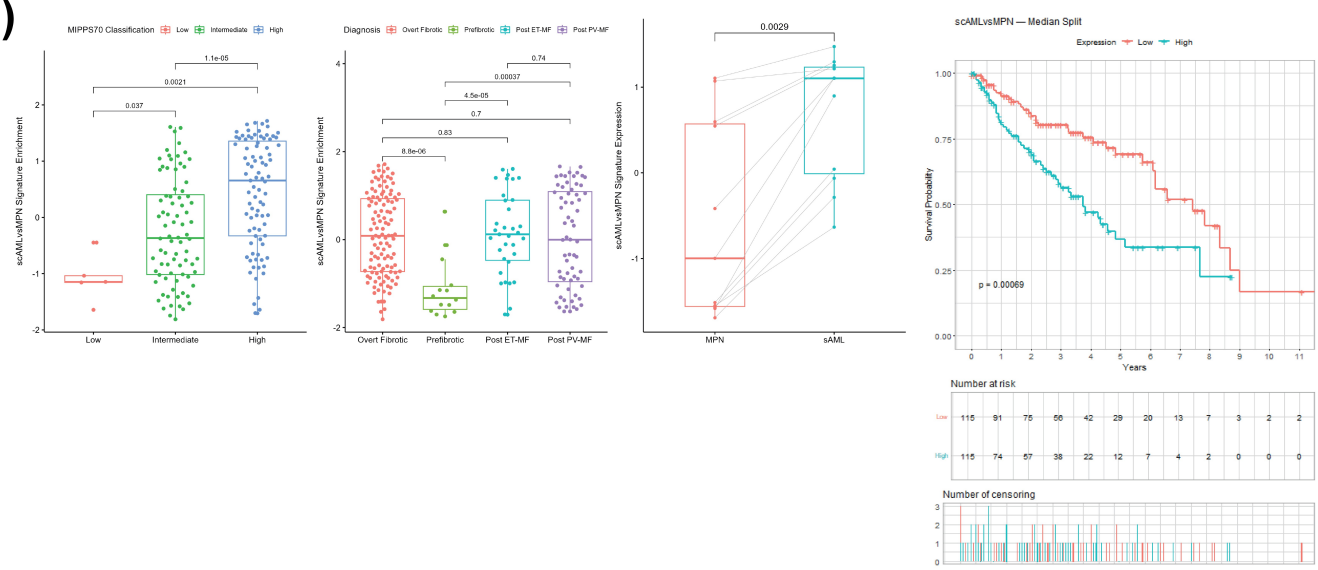
MIPPS70 Classification
Low
Intermediate
High
1.1e-05
0.0021
0.037
scAMLvsMPN Signature Enrichment
Diagnosis
Overt Fibrotic
Prefibrotic
Post ET-MF
Post PV-MF
0.74
0.00037
4.5e-05
0.7
0.83
8.8e-06
0.0029
MPN
sAML
scAMLvsMPN — Median Split
Expression
Survival Probability
p = 0.00069
Years
Number at risk
Number of censoring